



On the interference of Kr during carbon isotope analysis of methane using continuous-flow combustion–isotope ratio mass spectrometry

J. Schmitt¹, B. Seth¹, M. Bock¹, C. van der Veen³, L. Möller², C. J. Sapart³, M. Prokopiou³, T. Sowers⁴, T. Röckmann³, and H. Fischer¹

¹Climate and Environmental Physics, Physics Institute, & Oeschger Centre for Climate Change Research, University of Bern, Sidlerstrasse 5, 3012 Bern, Switzerland

²Alfred Wegener Institute Helmholtz Centre for Polar and Marine Research, Bremerhaven, Germany

³Institute for Marine and Atmospheric research Utrecht, Utrecht University, Princetonplein 5, 3584CC Utrecht, The Netherlands

⁴Earth and Environment Systems Institute, Penn State University, University Park, PA, USA

Correspondence to: J. Schmitt (schmitt@climate.unibe.ch)

Received: 12 January 2013 – Published in Atmos. Meas. Tech. Discuss.: 7 February 2013

Revised: 30 April 2013 – Accepted: 2 May 2013 – Published: 27 May 2013

Abstract. Stable carbon isotope analysis of methane ($\delta^{13}\text{C}$ of CH_4) on atmospheric samples is one key method to constrain the current and past atmospheric CH_4 budget. A frequently applied measurement technique is gas chromatography (GC) isotope ratio mass spectrometry (IRMS) coupled to a combustion-preconcentration unit. This report shows that the atmospheric trace gas krypton (Kr) can severely interfere during the mass spectrometric measurement, leading to significant biases in $\delta^{13}\text{C}$ of CH_4 , if krypton is not sufficiently separated during the analysis. According to our experiments, the krypton interference is likely composed of two individual effects, with the lateral tailing of the doubly charged ^{86}Kr peak affecting the neighbouring m/z 44 and partially the m/z 45 Faraday cups. Additionally, a broad signal affecting m/z 45 and especially m/z 46 is assumed to result from scattered ions of singly charged krypton. The introduced bias in the measured isotope ratios is dependent on the chromatographic separation, the krypton-to- CH_4 mixing ratio in the sample, the focusing of the mass spectrometer as well as the detector configuration and can amount to up to several per mil in $\delta^{13}\text{C}$. Apart from technical solutions to avoid this interference, we present correction routines to a posteriori remove the bias.

1 Introduction

Methane is the third most important greenhouse gas besides water vapour and CO_2 . The isotopic composition of atmospheric methane (CH_4) provides important constraints on globally integrated CH_4 sources and sinks (Kai et al., 2011; Levin et al., 2011). Both the concentration and the isotopic composition of atmospheric CH_4 in the past have been reconstructed from trapped bubbles in ice cores as well as from the interstitial air in snow pack (firn) on polar glaciers (Miller et al., 2002; Schaefer et al., 2006; Fischer et al., 2008; Sowers, 2011; Sapart et al., 2012). Originally, the dual-inlet technique coupled to an isotope ratio mass spectrometer (IRMS) was used (Stevens and Rust, 1982; Lowe et al., 1991). With the advent of the continuous-flow (CF) technique (Matthews and Hayes, 1978), a growing number of groups have developed systems that allow smaller quantities of CH_4 to be analysed, permitting routine analyses on ice core samples (Merritt et al., 1995; Rice et al., 2001; Miller et al., 2002; Ferretti et al., 2005; Sowers et al., 2005; Schaefer and Whiticar, 2007; Behrens et al., 2008; Umezawa et al., 2009; Melton et al., 2011; Sapart et al., 2011). An overview of these techniques is provided in Table 1. The general procedure for $\delta^{13}\text{C}$ - CH_4 analysis on air samples using the CF-IRMS technique usually involves several steps to separate a large number of major and trace atmospheric components (see general scheme in Fig. 1). For ice core samples, an additional extraction step

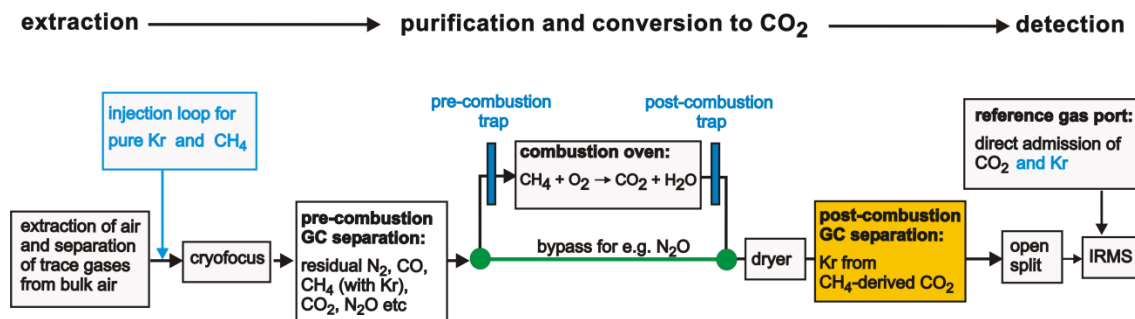


Fig. 1. Simplified flow scheme used for $\delta^{13}\text{C}$ analysis of CH_4 on air samples applying the continuous-flow IRMS technique. The scheme provides an overview of basic components and specific add-ons of the systems used in this study. The analysis comprises three main steps (from left to right: extraction, purification and combustion of CH_4 to CO_2 , and finally the detection in the isotope ratio mass spectrometer). The grey boxes represent the basic components used by all laboratories and date back to the milestone publications in this field (Merritt et al., 1995; Rice et al., 2001). An exception is the IMAU system described by Sapart et al. (2011), where no pre-combustion GC is used and the separation of the gases is achieved solely by a preconcentration step. Coloured symbols denote additional devices, which are specific for the certain laboratory. Blue and green colours denote features of the Bern system, while the yellow box is specific for the updated IMAU system. The injection loop (blue box) allows injecting pure CH_4 and Kr into the GC flow to monitor the system and allow special experiments. The pre-combustion trap and the post-combustion trap were included later on into the updated Bern system to remove the Kr interference. The yellow box represents the post-combustion GC, which was included in the updated IMAU system to remove the Kr interference.

either by dry or melt extraction has to be performed first. The purified CH_4 is then admitted to a combustion interface where CH_4 is converted to CO_2 , which is subsequently measured in the IRMS. Here, the most abundant isotopologues of CO_2 are measured using Faraday cups for the mass-to-charge ratios (m/z) 44, 45 and 46. From these ion beam intensities, the $\delta^{13}\text{C}$ of CH_4 is then calculated applying a correction for the isobaric contribution at m/z 45 due to the presence of $^{12}\text{C}^{17}\text{O}^{16}\text{O}$ (Craig, 1957).

The separation of CH_4 from the bulk air components (N_2 , O_2 and Ar) and also from minor components like CO is a delicate task. Usually, gas chromatography (GC) is used to separate CH_4 from CO, N_2 , and CO_2 , which would otherwise interfere with the mass spectrometric detection. In this respect, an interference with the atmospheric trace gas krypton (Kr) has not yet been considered during the method development. The noble gas krypton has a natural atmospheric abundance of 1099 ± 9 ppb (Aoki and Makide, 2005) and consists of many stable isotopes, with the most abundant being ^{84}Kr with 57% and ^{86}Kr with 17%. Although Kr is a trace gas, for several types of samples Kr levels are comparable or even higher than the corresponding CH_4 , e.g. for stratospheric samples (Rice et al., 2003; Röckmann et al., 2011) and air extracted from deep ice cores.

Since none of the Kr isotopes produces an ion that has exactly the same mass as the target ions with m/z 44, m/z 45 and m/z 46, Kr has not been regarded as an issue during $\delta^{13}\text{C}$ analysis of CH_4 until now. The physico-chemical properties of CH_4 and Kr are very similar, making them hard to separate from one another. Similar boiling points (Kr = 119 K and CH_4 = 111 K) make cryo-separation impossible, and gas chromatographic separation has proven to be very difficult. To ensure a sufficient separation of CH_4 from Kr, the GC

has to be operated at sub-ambient temperatures (Schüpbach et al., 2009) or at high flow rates ($50 \text{ mL STP min}^{-1}$) with a packed column at 25°C (Burford and Bremner, 1972).

Here we show that Kr actually does interfere with the measurement of $\delta^{13}\text{C}$ of CH_4 if Kr reaches the ion source together with the CO_2 peak derived from CH_4 combustion. The magnitude of the Kr interference depends on the preconcentration and GC separation of the Kr/ CH_4 mixture, the mass spectrometer and its source settings. We will show that the bias introduced by this interference can be as large as 2‰ when dealing with atmospheric samples with low CH_4 concentrations (< 400 ppb). More generally, for other types of samples, like water samples, these CH_4 concentrations correspond to CH_4/Kr ratios of < 0.5 . For atmospheric samples, the Kr interference scales with the atmospheric CH_4 mixing ratio since Kr is a well-mixed, inert constituent with an atmospheric mixing ratio that is assumed to vary by only $< 1\%$ between glacial and interglacial climate (Headly and Severinghaus, 2007; Ritz et al., 2011).

We demonstrate how this interference comes about and how this issue can be resolved. Initially, we discuss ways to identify Kr anomalies in chromatograms from $\delta^{13}\text{C}\text{CH}_4$ analyses. In the second part of the manuscript we highlight techniques to correct for the Kr interference and compare these techniques. This paper focuses only on the aspect of Kr interference during $\delta^{13}\text{C}$ analysis of CH_4 . However, based on the underlying mechanism of this interference we note that other IRMS applications might also be affected. This effect occurs in situations where a target species and a second species producing singly, doubly or triply charged ions with m/z close to the target masses are simultaneously present in the ion source due to co-elution or measurement of gas mixtures in dual inlet. For example Xe, which elutes in the vicinity of volatile

Table 1. Collection of publications dealing with $\delta^{13}\text{C}$ - CH_4 measurements in view of possible Kr interferences. The collection is not exhaustive and lists only some of the publications in the field of ice core and atmospheric measurements. To allow a faster orientation of which data set is produced by which method, we used the following scheme: technical paper (data paper).

Publication	Pre-combustion GC	Technical details and remarks
<i>dual-inlet techniques:</i> Stevens and Rust (1982) (Quay et al., 1999), Lowe et al. (1991) (Francey et al., 1999), Tyler et al. (1999) (Tyler et al., 2007) Bergamaschi et al. (2000)	No GC, only CO is removed prior to combustion. Therefore, all other organic compounds are combusted as well. However, ethane and other NMHC have low conc. compared to CH_4 , so the effect is small.	Prior to the conversion of CH_4 to CO_2 , atmospheric CO_2 is removed from the air stream. After the combustion unit, the produced CO_2 is trapped at LN_2 , thus separating it from Kr.
<i>continuous-flow techniques:</i> Merritt et al. (1995)	PoraPLOT Q, 25 m, 0.32 mm i.d., 20–25 °C, 1 mL min ⁻¹	no special measures to separate Kr from CH_4
Rice et al. (2001) (Rice et al., 2003)	PoraPLOT Q, 25 m, 0.32 mm i.d., GC temperature ramped from -50 °C to 30 °C, 2.6 mL min ⁻¹	GC with cryogenic unit to allow separation of CH_4 from an “unknown contaminant peak that otherwise interferes with masses 45 and 46”
Bräunlich et al. (2001)	MPI: Bergamaschi et al. (2000); LGGE: GS-Q, 30 m, 0.32 mm i.d.	The MPI data set is measured with dual inlet. For LGGE, Kr might co-elute with CH_4 .
Behrens et al. (2008) (Fischer et al., 2008)	CarbonPLOT, 30 m, 0.32 mm i.d., 30 °C, 1.1 mL min ⁻¹	no special measures to separate Kr from CH_4
Miller et al. (2002) (Ferretti et al., 2005; Bousquet et al., 2006)	Molecular Sieve 5A, 80 °C, 2.0 mL min ⁻¹	Separation of CH_4 and Kr on this column is unknown
Sowers et al. (2005) (Mischler et al., 2009)	PoraPLOT Q, 30 m, 0.32 mm i.d.	no special measures to separate Kr from CH_4
Schaefer and Whiticar (2007) (Schaefer et al., 2006)	GSQ PLOT, 30 m, 0.53 mm i.d., 0 °C, 1 mL min ⁻¹	Kr is separated from CO_2 by the post-combustion GC
Umezawa et al. (2009)	PoraPLOT Q, 25 m, 0.32 mm i.d., -30 °C, 3.0 mL min ⁻¹	GC with cryogenic unit to separate CH_4 from an unknown contaminant peak
Melton et al. (2011) (Melton et al., 2012)	GSQ PLOT, 30 m, 0.53 mm i.d., 25 °C, 1 mL min ⁻¹	post-combustion trap followed by an additional GC (GSQ PoraPLOT, 30 m, 0.53 mm i.d., 25 °C) separates Kr from CH_4 -derived CO_2
Brass and Röckmann (2010); Sapart et al. (2011) (Keppler et al., 2006; Vigano et al., 2009; Röckmann et al., 2011; Sapart et al., 2012)	No pre-combustion GC	Purification relies on preconcentration and cryofocus, as a replacement of the omitted pre-combustion GC

organic compounds, produces several triply charged ions in the m/z 44 to m/z 45 range, thus potentially interfering during carbon isotope analysis of trace gases that are measured as CO_2 .

Section 2 provides a brief overview on the setup of the four analytical systems where we identified the Kr interference. In Sect. 3, $\delta^{13}\text{C}$ - CH_4 chromatograms from the four analytical systems illustrate the common features and differences of the Kr interference. In Sect. 4, we describe tests that can be performed to determine if and to what degree Kr interferes in the chromatogram. Experiments were performed to assess the Kr impact on $\delta^{13}\text{C}$ - CH_4 analyses involving direct Kr injections

into the CF-IRMS and dual-inlet systems. It will be shown that the Kr interference affect all three Faraday cups. We then discuss the experimental results to illustrate just how the Kr interference works. Finally, Sect. 5 presents a suite of possible solutions to either separate Kr from CH_4 or CH_4 -derived CO_2 , or correct for this effect in existing data sets. While the paper is structured in these consecutive steps, the reader might profit from a first quick look at Figs. 3 and 7. Note that for practical reasons we use the term CH_4 peak, which corresponds to the CO_2 peak from the original CH_4 peak. Additionally, $\delta^{13}\text{C}$ denotes $\delta^{13}\text{C}$ of a CH_4 sample without specifying it.

2 Experimental setup and air samples

For the measurements and experiments described in this paper, we used four different analytical systems; they are named after the institutes or cities in which they were developed: AWI (Alfred Wegener Institute for Polar and Marine Research), Bern (University of Bern), IMAU (Institute for Marine and Atmospheric research Utrecht), and PSU (Penn State University).

2.1 AWI system

The AWI system is described in detail by Behrens et al. (2008) and was used to generate a $\delta^{13}\text{C}_{\text{CH}_4}$ data set covering the last deglaciation (Fischer et al., 2008) as well as a new data set covering the last glacial period (Möller et al., 2013). In short, the pre-purified CH_4 sample (together with Kr) is injected onto a 30 m CarbonPLOT column at 30 °C with a flow rate of ca. 1.1 mL min⁻¹. The detector is an Isoprime IRMS equipped with five Faraday cups: a universal triple collector for m/z 44, 45 and 46 to calculate $\delta^{13}\text{C}$ of CH_4 and two additional cups for m/z 28 and m/z 32 for monitoring the efficiency of the O_2 and N_2 separation of the trapping system. The five Faraday cups are connected to the following feedback resistors: $5 \times 10^8 \Omega$ (“N₂ cup”, m/z 28), $1 \times 10^9 \Omega$ (“O₂ cup”, m/z 32), $5 \times 10^8 \Omega$ (major m/z 44), $5 \times 10^{10} \Omega$ (minor1, m/z 45), and $1 \times 10^{11} \Omega$ (minor2, m/z 46).

2.2 Bern system

The Bern system is an updated and more versatile follow-up device compared to the AWI system, and its description is currently in preparation. While the AWI system is constructed to measure only $\delta^{13}\text{C}$ of CH_4 , the Bern system can analyse a larger suite of trace gases (CH_4 , N_2O and its stable isotopologues, xenon, ethane, propane, methyl chloride, CF_4). For that reason the Bern system is equipped with additional technical features allowing special experiments to be performed, e.g. a bypass valve for the combustion oven, and additional valves to inject CH_4 and Kr mixtures in helium (He) onto the GC system (Fig. 1). Like the AWI system, the Bern system uses a 30 m CarbonPLOT column, at 30 °C with a flow rate of ca. 1.0 mL min⁻¹. The Bern system uses an identical Isoprime IRMS to AWI, equipped with five Faraday cups: the raw data from the mass spectrometer measurements was processed using our in-house isotope software (Bock et al., 2010; Schmitt et al., 2011). After the identification of the Kr interference, two additional traps (pre-combustion trap and post-combustion trap) were installed to get rid of the Kr interference (Sect. 5.3). This new system is referred to as the updated Bern system.

2.3 IMAU system

A detailed description of the IMAU system is provided elsewhere (Brass and Röckmann, 2010; Sapart et al., 2011).

A special feature of this system is that it lacks the pre-combustion GC common in other systems (Fig. 1). The IMAU system uses a Thermo Finnigan Delta plus XL as detector. After the Kr interference was identified, the system was modified to remove the interference (Sect. 5.2). As shown in Fig. 1, a GC was added after the conversion of CH_4 to CO_2 (post-combustion GC), and this modified system is referred to as updated IMAU system.

2.4 PSU system

The measurements done at PSU use the system described earlier in Sowers et al. (2005). The mass spectrometer is a Finnigan MAT 252. Modifications to remove the Kr interference are in process.

2.5 Air samples

All four labs measured a set of three cylinders, which were part of an international round-robin study. These cylinders were filled at Niwot Ridge, Colorado, in 2007 to varying CH_4 concentrations with a balance of ultra-high-purity air (no CH_4) to mimic the pre-industrial period (PI, ~900 ppb), the last glacial period (GLA, ~380 ppb) and the present day (PD, 1870 ppb). The cylinders were then measured at NOAA to confirm the CH_4 values (GLA, cylinder no. CA01179 = 372 ppb; PI, cylinder no. CC71560 = 904 ppb; and PD, cylinder no. CA03560 = 1831 ppb). While the CH_4 concentration is different, the Kr concentrations of all cylinders should be at natural abundance (1099 ppb), as the GLA and PI cylinders were produced by diluting atmospheric air with CH_4 -free air. The three cylinders have the following CH_4 / Kr mixing ratios: 0.33 (GLA), 0.82 (PI) and 1.69 (PD), thus yielding CH_4 / Kr mixing ratios that vary by a factor of 5. Additionally, cylinder CA08289 (NOAA, Boulder) is used at Bern as a working standard containing 1508.2 ppb CH_4 , and IMAU used a natural whole-air working standard of Groningen (“GRO”) air with 1981.2 ppb CH_4 for the experiments where pure Kr is added.

3 First hints and visual inspection of chromatograms

The possible existence of an interfering compound during the IRMS analysis of $\delta^{13}\text{C}$ of CH_4 on air samples was first described in 2001 when Rice et al. (2001) described “an unknown contaminant peak”. As the contaminant could not be identified, it remained unclear if this was only a problem of their specific setup or if it is a general feature of air samples. We believe that this unknown contaminant peak was Kr. In hindsight, it is unfortunate that this interference was not resolved as subsequent groups that developed new systems for $\delta^{13}\text{C}$ analysis on CH_4 for air and ice core samples did not account for the Kr interference. This led to the current situation where many systems do not properly separate this “contaminant peak” from CH_4 , while others managed

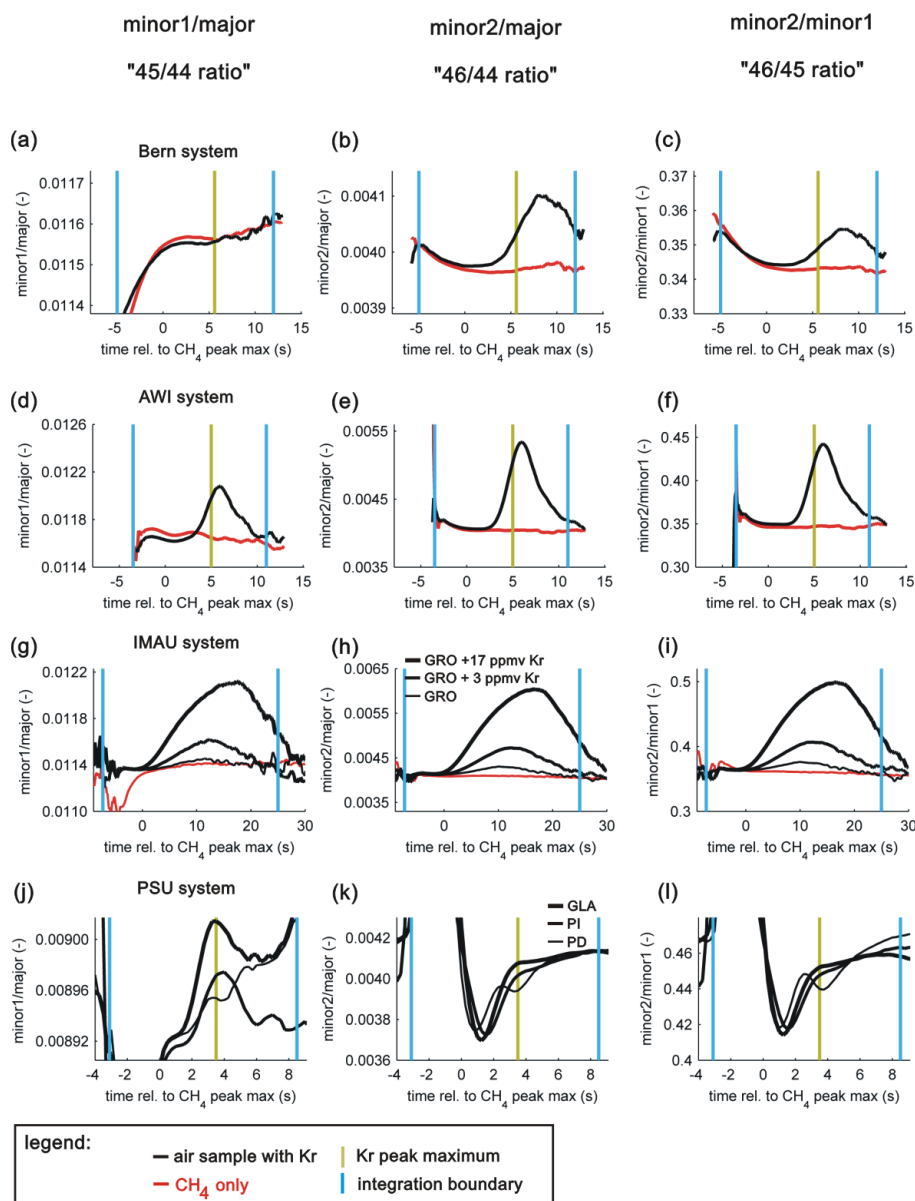


Fig. 2. Comparison of the ion current ratios of the four systems (from top to bottom: Bern, AWI, IMAU, PSU). The left column shows the minor1 / major ratio ("45/44 ratio"); the middle column shows minor2 / major ("46/44 ratio"), the right column minor2 / minor1 ("46/45 ratio"). Natural-air samples and air samples with added Kr are plotted as black lines, and injections of pure CH₄ are shown as red lines, illustrating the anomalies seen in the Kr containing samples. Blue vertical lines mark the left and right integration limits. Green vertical lines mark the maximum position of the Kr peak where we could determine its precise position. The Kr interference in the AWI system is visually more pronounced compared to the Bern system due to the differences in peak separation and focusing of the IRMS.

to separate this interfering substance (Schaefer and Whiticar, 2007; Umezawa et al., 2009; Melton et al., 2011).

The search for an interfering substance during $\delta^{13}\text{C}$ analysis of air samples was started during the interlaboratory calibration exercise involving both air cylinders and glacial ice samples (see results in Table 2). The observed $\delta^{13}\text{C}$ differences scaled with CH₄ mixing ratios and were as large as 2 ‰ for low CH₄ samples (e.g. CH₄ < 400 ppb). While the co-

elution of CH₄ and Kr and the generation of a m/z 43 peak due to $^{86}\text{Kr}^{2+}$ was recognised during the development phase of the Bern system, it was the addition of Kr to a natural-air sample (GRO) at IMAU that confirmed the Kr interference on $\delta^{13}\text{C}$. The effects on the measured $\delta^{13}\text{C}$ and $\delta^{18}\text{O}$ values were significant and scaled linearly with the Kr amount added. For each 1 ppm Kr addition, the $\delta^{13}\text{C}$ values and $\delta^{18}\text{O}$ values of the spiked air sample shifted by 0.79 ‰ and by

Table 2. Collection of $\delta^{13}\text{C}\text{-CH}_4$ results from the interlaboratory calibration round robin. As described in Sect. 2.5 these three cylinders with contrasting CH_4 mixing ratios are referred as GLA, PI, and PD. For some results Kr correction was applied using the following methods: ^a using the approach described in Sect. 5.4, and ^b according to Sect. 5.6. Besides the NIWA (National Institute of Water & Atmospheric Research) lab, which measured the cylinders with dual-inlet IRMS measurement and CF-IRMS, all results were obtained using CF-IRMS. The NIWA dual-inlet data were measured according to Lowe et al. (1999), and Kr would have been pumped away once CO_2 (from CH_4) was recovered from the combustion step. These values should be regarded as close to the true values. The NIWA CF-IRMS data were obtained using the method described in Miller et al. (2002) but used a CP-PoraBOND Q column ($50 \times 0.32 \text{ mm} \times 5 \mu\text{m}$ at 40°C) instead of the Molecular Sieve 5A column at 80°C used in the original publication. Ideally, the NIWA dual-inlet results and the values after Kr correction should be the same within their common error. Deviations among the results are the sum of differences due to referencing standards, amount effects, and imperfect Kr correction.

Cylinder name [CH_4]	GLA 372 ppb		PI 904 ppb		PD 1831 ppb	
	mean	1σ	mean	1σ	mean	1σ
$\delta^{13}\text{C}\text{-CH}_4$ ($\% \text{ VPDB}$)						
PSU as measured	-46.86	0.06	-47.15	0.10	-47.08	0.16
PSU Kr-corrected ^a	-47.52	0.06	-47.41	0.10	-47.20	0.16
Bern as measured	-47.31	0.11	-47.37	0.07	-47.41	0.09
AWI as measured	-46.25	0.11	-47.07	0.09	-47.14	0.05
AWI Kr-corrected ^a	-47.06	0.13	-47.40	0.12	-47.32	0.06
NIWA dual inlet	-47.43	0.02	-47.44	0.02	-47.23	0.02
NIWA CF as measured	-46.52	0.08	-47.78	0.20	-47.02	0.15
IMAU old method	-44.82	0.33	-46.64	0.13	-47.22	0.11
IMAU Kr-corrected ^b	-47.18	0.24	-47.43	0.11	-47.26	0.05
IMAU updated method	-47.20	0.20	-47.52	0.11	-47.27	0.07

7.2 ‰ towards heavier values, respectively. This experiment clearly showed that Kr did interfere and could explain a large part of the discrepancies between the labs. However, it was unclear whether the observed effect was specific for this system or if other systems were affected as well. Additionally, the nature of this interference had to be elucidated in order to come up with technical solutions and correction routines for older data sets.

Since the ion current intensities of this interference are difficult to visualise in the chromatograms themselves, we chose to use the ratio of ion currents to identify the position of the Kr peak relative to the CH_4 peak. Commercial IRMS software packages usually provide graphs of the ion current ratios only for the measured total ion current ratios, i.e. the combined intensities for the sample peak and the background. When the interference in one of the ion current ratios is very pronounced, it is possible to identify it in the total ion current ratios (Rice et al., 2001; Schaefer and Whiticar, 2007). This is the case when the CH_4 and the interference peak are chromatographically well separated. However, when the two peaks strongly overlap, the influence is less visible. A more sensitive way to identify such interferences in chromatograms is to inspect ion current ratio plots where the background signal has been subtracted from the measured signal to yield the signal of the sample peak only. The plots of this paper show ion current ratios which were corrected for the background signal. Figure 2 shows the three ion current ratios for the time interval around the CH_4 peak.

The retention time of the CH_4 peak maximum is defined as 0 s. Throughout the paper we label the three ion current ratios according to the involved Faraday cups and the m/z of the ions which are commonly detected in this cup at CO_2 focusing: minor1 / major (“45/44”), minor2 / major (“46/44”), and minor2 / minor1 (“46/45”). Note the m/z pairs are put in parenthesis (e.g. “45/44”) to indicate that only the target ions produced by CO_2 strictly adhere to this rule. It will be shown in this paper that a small fraction of the m/z 43 beam ($^{86}\text{Kr}^{2+}$) tails all the way into all three cups (major, minor1 and minor2). For the Bern, AWI and IMAU systems, air samples containing Kr (Fig. 2 black lines) are compared with pure- CH_4 samples (Fig. 2 red lines). For the systems where it was explicitly determined (see below and Figs. 3 and 4), the position of the Kr peak relative to the CH_4 peak is marked for orientation. As can be seen for all four systems, most ion current ratios of samples containing Kr deviate from the ratios of pure CH_4 . While these anomalies are well pronounced in all three ratios for the AWI system and resemble a Gaussian shape, the Bern system exhibits no visible anomaly for the “45/44 ratio”, which will be discussed later. In the IMAU case, where Kr was added to natural air in increasing amounts, one sees that the anomalies become larger with more Kr added. Note that the large anomalies are only the result of large amounts of Kr to an air sample (3 times or 17 times the Kr amount of a natural sample (GRO)). The anomalies of the natural-air sample (GRO) are small and hard to detect without prior knowledge. In the

case of the PSU system, an anomaly is only barely visible for the “45/44 ratio” and obscured by the internal fractionation within the peak (time shift due to mismatch of the resistor–capacitor pair). In conclusion, the visual inspection of the ion current ratios of all four systems points to an interfering substance present in natural-air samples. The appearance of this anomaly is specific for each of the four systems and depends on chromatographic separation and properties of the IRMS itself. These anomalies in the ion current ratios can be hidden especially when the background is not subtracted. It requires a careful comparison of the ratios from the natural-air sample with those from pure CH₄ to recognise this matrix effect.

4 Experiments and results

4.1 Simple experiment to identify Kr in the chromatogram

The visual inspection of the chromatograms described above revealed that an interfering compound that we believe is Kr produces anomalies in the ion current ratios. Here we go one step further and provide a test to identify whether the retention time of Kr overlaps with the CH₄ peak. As mentioned above, the behaviour of Kr and CH₄ on GC columns is similar and can result in overlapping peaks with Kr eluting only a few seconds after CH₄. The following experiment uses the fact that, for the electron energies used in the ion source of the IRMS (e.g. 80 eV for the Bern system), ions with two (and sometimes three) electrons removed are also produced (Denifl et al., 2002; King and Price, 2008). Since the optical system of the IRMS separates ions according to their mass-to-charge ratio (m/z), heavy isotopes like ⁸⁶Kr can be readily transformed into m/z 43 ⁸⁶Kr²⁺ ions that strike the imaging plane close to the major ion Faraday cups. Therefore, ⁸⁶Kr²⁺ ions can be easily monitored by shifting the accelerating voltage (AV) to higher values, e.g. 4030 V instead of 3975 V for the CO₂ focusing for the Bern Isoprime, so that the m/z 43 ⁸⁶Kr²⁺ ions are detected in the m/z 44 cup. The m/z 43 beam (⁸⁶Kr²⁺) falls into the major cup, while the m/z 45 beam (mostly ¹³C¹⁶O¹⁶O) falls into minor2, monitoring the position of the CH₄ peak. This focusing test has the advantage that it can be run on any system with any natural-air sample without modifications to the CH₄ separation system. The results of these focusing experiments are shown in Fig. 3. As can be seen in Fig. 3a, the chromatographic separation of CH₄ from Kr is about 6 s for the Bern system. Since the peak width (FWHM) for both CH₄ and Kr is also 5–6 s, both peaks do overlap considerably (Fig. 3a), but the overlap is system dependent. From this experiment we can derive the following conclusions. First, a considerable amount of doubly charged Kr ions are produced within the source of the IRMS. Second, ⁸⁶Kr²⁺ ions allow identifying the retention time of Kr and illustrate that the GC conditions of the Bern and PSU systems are insufficient to separate Kr from CH₄. Third, the position

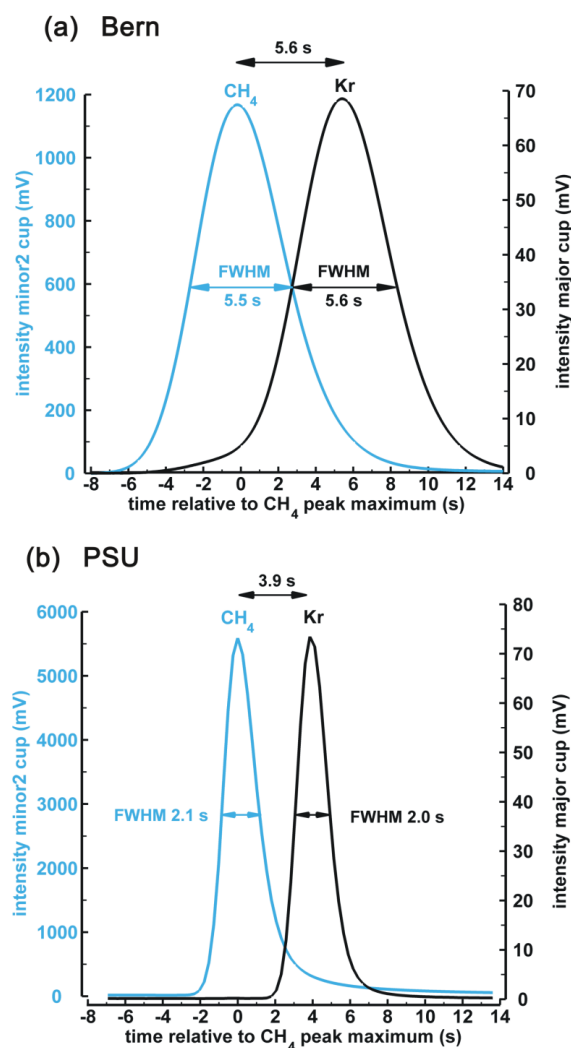


Fig. 3. Chromatogram of an atmospheric air sample showing the separation of CH₄ from Kr for the Bern system (a) and the PSU system (b). The ion source of the IRMS was focused such that the m/z 43 beam of ⁸⁶Kr²⁺ falls into the major cup (black line, right axis). The isotopologues of CO₂ with m/z 45 fall into the minor2 cup and mark the position of the CH₄ peak (blue line, left axis).

of the Kr peak and the observed anomalies seen in the ion current ratios (Fig. 2) are similar and suggest that Kr causes these anomalies.

4.2 Injections of pure Kr into GC flow

The visual peak inspection and the overlap of CH₄ and Kr from the focusing exercise point to Kr as the source of the interference. However, at this stage it remains unclear how Kr might interfere with the $\delta^{13}\text{C}$ measurement since a direct isobaric effect seems unlikely as none of the Kr isotopes are expected to fall into the given Faraday cups at their nominal m/z as singly or doubly charged ions. Several studies report on non-isobaric interferences during stable isotope analysis

of gas mixtures without a clear hint of the mechanisms behind them (Mariotti, 1984; Sarma et al., 2003). One possible mechanism generating our anomalies could be that the presence of Kr in the ion source changes the relative ionisation efficiency of the CO₂ isotopologues in the sense of “ionisation quench” coined by Meier-Augenstein et al. (2009). In dual-inlet applications such matrix interactions of gases in the ion source are commonly termed “chemical slope” (Severinghaus et al., 2003) and refer to differences in the composition of sample and standard gas mixture. While correcting for this effect is common practice, the underlying processes in the ion source are poorly understood.

Alternatively, Kr itself without any interaction with CO₂ produces the observed signals. A simple test to distinguish between these two possibilities is the injection of pure Kr. If the pure Kr does not produce a positive signal by itself, then the interference relies on the interaction of CO₂ and Kr in the ion source. In contrast, if Kr alone generates these signals, then some of the Kr ions are deflected from their expected flight path to fall into Faraday cups with m/z values up to 3 units higher.

To perform this experiment a mixture of pure Kr in He was injected via the injection loop into the GC flow of the Bern system (see Fig. 1). The amount of injected Kr roughly equals the amount of Kr of ca. 10 mL STP natural air; thus, a similar amount as is used in our routine ice core measurements. The injected Kr is cryofocused first and then sent to the pre-combustion GC (Fig. 1). After the Kr peak left the GC, the flow passes a dryer before admitting it to the ion source of the IRMS (operated at CO₂ configuration). Note that the combustion oven is bypassed in this experiment to prevent the generation of a small CO₂ peak from trace amounts of residual CH₄ present in the He flow. The results of this experiment are shown in Fig. 4, together with the measurement of a natural-air sample. Kr itself produces signals in all Faraday cups at a retention time of ca. 6 s after the usual CH₄ peak maximum (Fig. 4c). This result supports the idea that Kr alone produces the signals detected in the three cups. A comparison with the signal intensities of the air sample (Fig. 4a) shows that the Kr intensities are clearly too small to be directly seen in the air sample itself; e.g. for the minor2 cup, the Kr signal is 4 mV at its maximum while for the air sample, the minor2 signal at the same time is ten times higher. Besides these two basic features, the experiment with pure Kr affords us the opportunity to investigate the general features observed in the ion current ratios of the air sample. A combusted CH₄ sample produces signal intensities (mV) in the three Faraday cups reflecting the natural abundance of the CO₂ isotopologues. For example, the signal of the major cup is a bit higher than the minor2 signal (Fig. 4a). In contrast, Kr produces a 4-times-higher minor2 signal compared to the signal on the major cup (Fig. 4c). In other words, the signals produced by Kr have a very different isotopic fingerprint compared to the CO₂ signals. In this example dealing with minor2 vs. major cup (“46/44 ratio”),

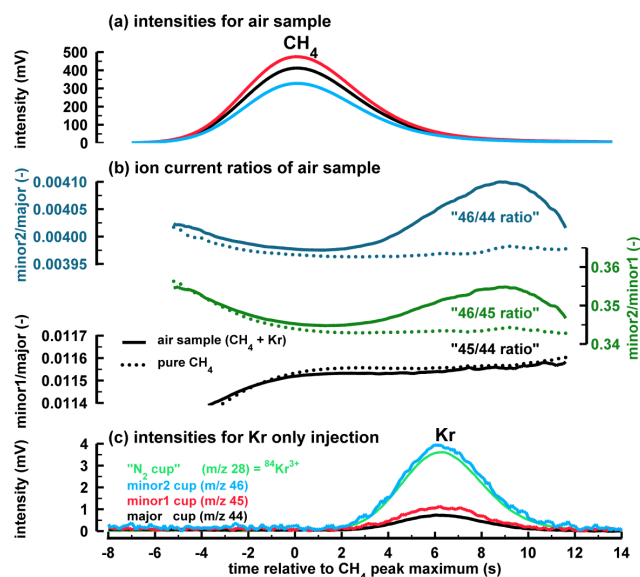


Fig. 4. Comparison of a CH₄ peak of an air sample with the signals gained from an injection of pure Kr measured with the Bern system at CO₂ focusing. **(a)** Beam intensities in mV for the CH₄ sample peak (369 ppb CH₄ with natural abundance of Kr) with the retention time centred to the CH₄ peak maximum. **(b)** Background-corrected ion current ratios (“46/44 ratio” in blue, “46/45 ratio” in green and “45/44 ratio” in black) of the atmospheric air sample (solid line) and pure CH₄ (dotted line), illustrating the anomalies seen in “46/44” and “46/45” but with no visible effect on “45/44”. Panel **(c)** shows the beam intensities for a measurement where Kr was injected into the GC flow. Due to the chromatographic effect of the GC column, the retention time of the Kr peak is ca. 6 s longer than the CH₄ peak, yet there is a considerable overlap. Note the signal measured at m/z 28 (“N₂ cup”) can be directly related to ⁸⁴Kr³⁺, which has the exact value of m/z = 28.

the Kr signals translate into a very heavy apparent $\delta^{18}\text{O}$ signature since the $\delta^{18}\text{O}$ is mainly determined by the “46/44 ratio”. When such an anomaly is added to the signals from combusted CH₄, the observed “46/44 ratio” will increase as it is the case for the air sample (Fig. 4b, “46/44 ratio”). In contrast, the minor1/major ratio of both the air sample and Kr are comparable, with the signal on minor1 being slightly higher than on major (Fig. 4a and b). Consequently, the signals created by Kr do not produce a visible anomaly in the minor1/major ratio as the “45/44 ratio” of the air sample closely follows the ratio of pure CH₄ (Fig. 4b “45/44 ratio”). Note that this close match of the “45/44” signature of Kr and CO₂ is just a coincidence and only observed for the Bern system. The other three systems show anomalies in the “45/44 ratio” (Fig. 2), which translate into too-heavy $\delta^{13}\text{C}$ values for natural-air samples as well. In addition to the more direct influence of the “45/44” anomaly on $\delta^{13}\text{C}$, the “46/44” anomaly also alters $\delta^{13}\text{C}$ of CH₄ samples. This is due to the fact that the ¹⁷O correction algorithm (Craig, 1957; Santrock et al., 1985) relies on assumptions regarding

the natural proportions of the stable oxygen isotopes, i.e. the relative contribution of ^{17}O ($^{12}\text{C}^{17}\text{O}^{16}\text{O}$ with m/z 45) and ^{18}O ($^{12}\text{C}^{18}\text{O}^{16}\text{O}$ with m/z 46), which are violated by the Kr signals.

4.3 Injection of pure Kr at varied accelerating voltage

The previous experiments clearly showed that Kr is responsible for the observed effects; yet, the underlying mechanism cannot be unambiguously derived from these experiments. Because the m/z 43 beam produced by $^{86}\text{Kr}^{2+}$ is only a few m/z units away from the target signals at m/z 44, m/z 45 and m/z 46, we propose two hypotheses. The first hypothesis assumes that the observed signals detected in the three Faraday cups are caused by ions with a mass-per-charge ratio corresponding to the nominal m/z of the cups, i.e. m/z 44, m/z 45 and m/z 46. Since ions with m/z 43 are available in the source, one might assume that light gases or their ions (e.g. He, H_2 or H) might react with $^{86}\text{Kr}^{2+}$ ions to form molecules or adducts (Leckrone and Hayes, 1998; Sessions et al., 2001), which then could provide the necessary m/z 44, m/z 45 and m/z 46 signals. The other hypothesis assumes scattering processes lead to broader m/z distributions, e.g. that the lateral tail of the m/z 43 beam ($^{86}\text{Kr}^{2+}$) extends all the way to m/z 46, thus covering 3 m/z units. The fact that the major ion beam contributes some intensity to the neighbouring minor was already observed during the early days of dual-inlet IRMS and termed “pressure effect” or “pressure broadening” and has been treated with abundance sensitivity corrections (Deines, 1970; Mook and Grootes, 1973; Fallick and Baxter, 1977). Peak-tailing effects are also of concern during clumped-isotope analysis of CO_2 where far reaching tails of the major beam on the distant minor beams have been investigated (He et al., 2012). A peak-tailing effect was also observed during stable-sulphur analysis using SF_6 , giving rise to an abundance sensitivity correction to prevent scale compression and accuracy problems (Ono et al., 2006). However, in these cases it is the regular major beam which contributes intensity to the minor beam and not a contaminant species like Kr as assumed in our case. Figuring out the actual process leading to this interference is not only helpful in understanding the different phenomena seen in the four investigated systems, but also in making assumptions about the stability of this interference over time and its sensitivity to changes in focusing parameters, etc. These characteristics are important for developing robust correction routines on existing data sets.

To explore the nature of the interference in more detail we conducted two different experiments where the ion current intensities are monitored as a function of the AV. In the first experiment, Kr was repeatedly injected into the GC flow, while the AV was slightly changed after each injection. In a second experiment, Kr was continuously admitted to the ion source through a capillary, while the AV was changed over a wide range.

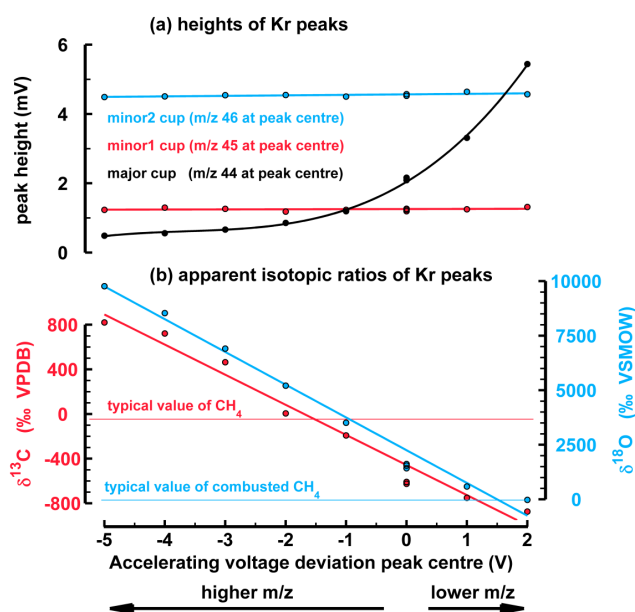


Fig. 5. Influence of slight changes in the accelerating voltage on the peak heights and apparent isotopic signatures of Kr peaks. Results of Kr injection into GC flow carried out with the Bern system with the source focused to CO_2 . (a) The upper panel shows the measured peak heights for the three Faraday cups (major, minor1, minor2) of the Kr peak as a function of the accelerating voltage; dots represent measurements and lines a linear fit for minor1 and minor2, and a cubic fit for the major cup. (b) The lower panel shows the apparent isotopic composition ($\delta^{13}\text{C}$ in red and $\delta^{18}\text{O}$ in blue) of the Kr interference calculated from the peak area of the Kr peaks; dots represent measurements and lines the linear fits.

4.3.1 Kr injections onto GC flow at varied accelerating voltage

In the following experiment pure Kr was repeatedly (10 times) injected into the GC flow of the Bern system and cry-focused prior to GC separation. The amount of injected Kr roughly matches the Kr amount of a 10 mL air sample to provide realistic measurement conditions. Measurements were conducted using the CO_2 configuration, but after each Kr peak the AV of the ion source was slightly changed to cover a range from -5 V to $+2$ V relative to the peak centre (PC) value of the CO_2 focusing. Each Kr peak is preceded by a rectangular CO_2 peak from the reference port (“standard on-off type”) and measured at the same AV to monitor the effect on the $\delta^{13}\text{C}$ and $\delta^{18}\text{O}$ values of CO_2 . Since the applied AV variations cover less than 0.1 m/z unit, the ion beams still fall into their respective Faraday cups. As a consequence, the $\delta^{13}\text{C}$ and $\delta^{18}\text{O}$ values of the rectangular CO_2 peaks are only slightly affected by these AV shifts (ca. 2‰ for both $\delta^{13}\text{C}$ and $\delta^{18}\text{O}$, data not shown). In contrast, the maxima of the Kr peaks in the major cup (m/z 44 at PC) increase from ca. 0.5 mV to almost 6 mV, i.e. a factor of 12 as the AV is increased from -5 V to $+2$ V (Fig. 5a). Since the peak heights

and areas for minor1 (m/z 45 at PC) and minor2 (m/z 46 at PC) remain fairly constant, the apparent isotopic ratios $\delta^{13}\text{C}$ and $\delta^{18}\text{O}$ of the Kr peaks show huge changes, reflecting these drastic changes in the beam ratios (Fig. 5b). We calculated these apparent $\delta^{13}\text{C}$ and $\delta^{18}\text{O}$ values by integrating the peak areas of the tiny Kr peaks for the three cups and applied the same algorithm as if they were CO_2 peaks. Our interpretation is that by increasing AV, the amount of $^{86}\text{Kr}^{2+}$ falling into the major cup quickly increases since the steep tail of this m/z 43 beam is moved closer to the edge of the major cup. The observation of this strong intensity increase on the major cup thus rules out the notion of an ion with m/z 44 producing this interference. However, for the rather constant intensities measured on minor1 and minor2 this experiment cannot rule out the existence of an ion at m/z 45 or m/z 46 since the AV changes were too small to move the centred beam out of the Faraday cup, as can be inferred from the rather constant $\delta^{13}\text{C}$ and $\delta^{18}\text{O}$ values of the CO_2 rectangular peaks (data not shown) and illustrated in Figs. 6 and 7.

Apart from identifying the nature of this interference, this experiment provides valuable information regarding the effects of the Kr interference during sample measurements. From Fig. 5 it is obvious that the apparent $\delta^{13}\text{C}$ or $\delta^{18}\text{O}$ signatures of the Kr interference are not constant but depend on the peak centre setting. Consequently, the influence of Kr on the calculated $\delta^{13}\text{C}$ values of CH_4 samples is not a constant property for any instrument, but both the sign and the magnitude of this effect are sensitive to the setting and stability of the source. As an example, at an AV offset of -1.5 V with respect to the peak centre, the apparent $\delta^{13}\text{C}$ value of the Kr interference intersects with the range of $\delta^{13}\text{C}$ values typical for natural CH_4 samples (around -40 to -70 ‰, red horizontal line in Fig. 5b). If samples are measured at this AV setting, then the Kr effect on $\delta^{13}\text{C}$ of CH_4 will be relatively small and hard to detect. However, for AV offsets < -1.5 V the measured $\delta^{13}\text{C}$ values will be heavier, and for AV offsets > -1.5 V $\delta^{13}\text{C}$ will become progressively lighter. For $\delta^{18}\text{O}$, the Kr bias will always push towards higher values. Note that these values are specific for a certain focusing of a specific instrument. How subtle differences can produce very different effects can be seen in the results of the AWI and Bern instruments, which have identical IRMS. The AWI system shows a pronounced effect in “45/44” (i.e. $\delta^{13}\text{C}$), while the effect on “45/44” for the Bern instrument is small (compare Fig. 2a and d). Usually, the AV at peak centre is determined automatically during the peak centre procedure; thus the bias could be relatively constant for a certain focusing. However, after performing a peak centre its actual position can move by up to 1 V over the course of hours, thus generating a time-dependent bias on the $\delta^{13}\text{C}$ values during a measurement, which will add noise to the data set. On the other hand, the close relationship between apparent $\delta^{13}\text{C}$ and $\delta^{18}\text{O}$ values provides a means to correct biased $\delta^{13}\text{C}$ measurements if the expected $\delta^{18}\text{O}$ value of a sample can be predicted or assumed with good precision. This situation often holds for $\delta^{13}\text{C}$ since

the $\delta^{18}\text{O}$ value of the CH_4 -derived CO_2 is not dependent on the CH_4 sample but set by the O_2 used during the combustion process. Therefore, the tight $\delta^{18}\text{O}$ – $\delta^{13}\text{C}$ correlation seen in Fig. 5b can be used to correct samples which are affected by the Kr interference (see Sect. 5.6).

4.3.2 Admission of Kr into the ion source at varied accelerating voltage

The aim of the following experiments is to better characterise the Kr interference using a wider m/z range.

To better understand an AV scan with pure Kr, we first present an AV scan for CO_2 (Fig. 6a). For practical reasons, the cups of the triple collector unit (universal collector) of most manufacturers have different widths (resolving slit width) to accommodate multipurpose usage, e.g. $\delta^{15}\text{N}$ of N_2 , $\delta^{18}\text{O}$ of O_2 . For the Bern IRMS, an AV change of 85 V is roughly equivalent to 1 m/z difference in this mass range. Figure 6b shows the ion current intensities for the three cups in fA for the same AV scan, but with Kr being admitted to the ion source. The $^{86}\text{Kr}^{2+}$ ion beam with nominally m/z 43.0 starts to fall into the major cup at around $+5$ V and reaches plateau intensity at $+20$ V (“transition zone”) with around 600 000 fA (Fig. 6b bottom panel). Zooming into the major signal reveals that after the initial steep drop to the left of the transition zone (towards higher m/z), the intensity only gradually decays when moving to -90 V, i.e. corresponding to ions with a nominal m/z of already 45 (see Fig. 6a with 85 V corresponding to about 1 m/z unit). The continuation to even-higher m/z is visible in the signal of minor1, where the intensity decreases from ca. 80 fA at $+60$ V (corresponding to ca. m/z 44.7) to ca. 30 fA at -90 V (corresponding to ca. m/z 46.0). Similarly, the continuation is visible in minor2, where the Kr signal becomes almost flat at around 80 fA, covering a range of m/z 45.7 to m/z 47.0. The fact that Kr produces higher intensities for minor2 compared to minor1 reflects the contrasting widths of the two cups: the wider minor2 cup collects Kr ions from a larger m/z range than the smaller minor1 cup (see also scheme of Fig. 7). Again, it is obvious that very small changes in the choice of the peak centre position can have a large effect on the apparent $\delta^{13}\text{C}$ and $\delta^{18}\text{O}$ signature of the Kr interference as already seen in Fig. 5b. Further, the flatness of the Kr signal in the region of m/z 45 and m/z 46 explains the strong linear correlation of $\delta^{13}\text{C}$ and $\delta^{18}\text{O}$ seen in the other experiments and measured air samples and is the basis for one of the correction methods explained below which rely on a linear relation of the m/z 45 and m/z 46 biases.

4.4 Summary of experiments and concept of Kr interference

Figure 7 shows a schematic drawing which illustrates the involved Faraday cups and the positions of the respective ion beams for CO_2 and $^{86}\text{Kr}^{2+}$ as well as the two effects which

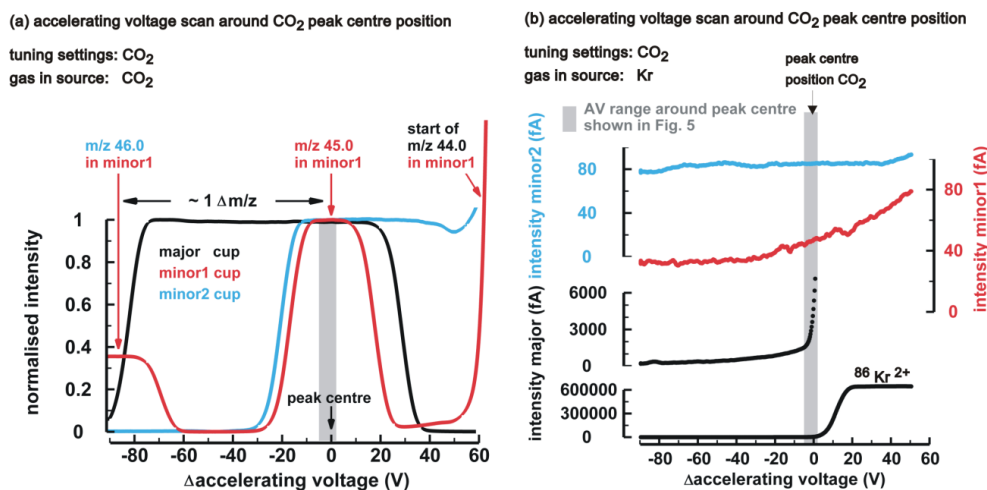


Fig. 6. Accelerating voltage (AV) scans around the peak centre position of CO₂ measured with the Bern system. The plots show beam intensities as a function of ΔAV , i.e. the differences to the AV at peak centre position at 3975 V. **(a)** AV scan with CO₂ from the reference port with normalised beam intensities for the three Faraday cups. The different peak widths reflect the geometric widths of the cups from small (minor1) to intermediate (minor2) to wide (major). **(b)** AV scan with Kr admittance by an additional valve at the Isoprime ref gas box showing the evolution of the Kr interference over a wide m/z range covering all three Faraday cups. The intensities are plotted in fA, thus, proportional to the number of ions collected in the cup. For the major cup, the full range is shown in the bottom panel covering the plateau (600 000 fA at $\Delta AV > 20$ V). The zoomed version of the major cup allows a better inspection of this signal decay to values < 1000 fA. The intensity of the Kr signal decays further in the m/z 45 region, as monitored by the minor1 cup and becomes almost flat at around m/z 46 (minor2 cup). Note the intensities measured with the minor2 cup are ca. factor 2 higher than for minor1 mirroring the different widths of the two cups.

might contribute individually to the observed Kr signals. For the construction of the Kr signals shown in the lower panels (Fig. 7b and c) we used the measured data of Figs. 5 and 6 and the interpretation we derive from these experiments. It is clear from Fig. 6b that most ions are well focused into a sharp beam with steep flanks as intensity rapidly drops to $< 1/1000$ of the plateau level for a 15 V shift in the accelerating voltage, corresponding to about 0.2 m/z units. Only the close-by major cup is strongly affected by this broadening effect. This rapidly dropping signal close to the beam centre can be attributed to the abundance sensitivity effect (Deines, 1970). We refer this contribution of the total Kr signal as the $^{86}\text{Kr}_{\text{tail}}^{2+}$ since it corresponds to the lateral tail of the proper $^{86}\text{Kr}^{2+}$ beam (light green curve Fig. 7b). However, the remarkable feature of the measured Kr signal is that this drop does not continue its rapid drop but decays only very slowly and finally becomes flat when its intensity reaches about $1/10,000$ of the plateau signal at the 20 V distance from the plateau edge (Fig. 6b). This observation is not predicted by abundance sensitivity because in that case the signal far out of the beam centre (the region of minor1 and especially minor2 cup) should drop more rapidly. One option to produce such an elevated background for higher masses far from the beam centre is that ions must have experienced a higher accelerating energy in the ion source. The other option would be interaction or scattering of $^{86}\text{Kr}^{2+}$ ions with He, thus energy loss, after the ions passed the magnetic field. It is also

conceivable that this flat contribution might be unrelated to the $^{86}\text{Kr}^{2+}$ beam, but originate rather from unspecific, broad scattering of the more abundant singly charged Kr ions. For example, filament or ion source processes could produce a broad distribution of low-energy Kr^+ ions which then lead to a broad field of ions with apparent m/z in the range the CO₂ target masses. Likewise, Kr^+ ions could hit the flight tube and produce a field of secondary ions which reach the Faraday cups indirectly. We name this flat contribution $\text{Kr}_{\text{scatter}}$ (brown line in Fig. 7b).

Figure 7c shows the sum of both contributions ($^{86}\text{Kr}_{\text{tail}}^{2+}$ and $\text{Kr}_{\text{scatter}}$) resembling the general features of our experiments and illustrates the Kr interference. While the ion density of the total Kr signal gradually declines further away from the peak maximum at m/z 43, the transformation from the ion current (apparent fA unit) to the voltage unit (apparent mV unit) overcompensates this drop (Fig. 7c). As a consequence, the signals (on an apparent mV unit) gained from minor1 and minor2 are higher compared to the major signal. The signal intensities are spatially integrated according to the width of the Faraday cups: the wider the cup, the more ions from the tail are collected. Accordingly, the integrated signal from minor2 is higher than the integrated minor1 signal. In summary, the Kr interference signal of a certain Faraday cup is not only a function of the ion flux at this position along the optical plane, but also depends on the width of the Faraday cup.

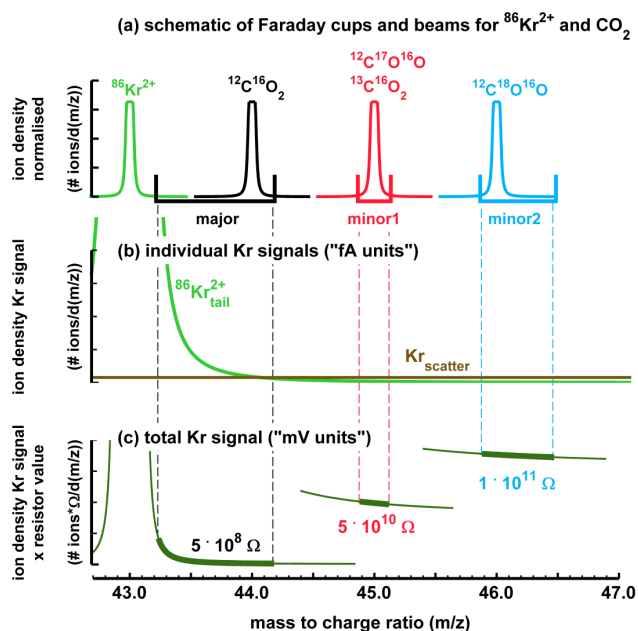


Fig. 7. Schematic showing the Faraday cups and the involved ion beams of CO_2 and the contribution from Kr to help visualise the observed Kr interference during $\delta^{13}\text{C}$ analysis as observed with the Bern IRMS. **(a)** Estimated positioning and width of the Faraday cups and the position of the respective ion beams (m/z) of the CO_2 isotopologues and $^{86}\text{Kr}^{2+}$. **(b)** Individual contributions from Kr. To illustrate the tailing of the m/z 43 $^{86}\text{Kr}^{2+}$ beam ($^{86}\text{Kr}^{2+}_{\text{tail}}$, light green) into the major cup, an artificial density distribution is used to provide a reasonable lateral distribution. The broad, unspecific part of the Kr interference, $\text{Kr}_{\text{scatter}}$, is illustrated by a brown horizontal line. **(c)** The sum of the two Kr contributions is plotted in dark green, but ion densities were converted to a mV unit using the respective values of the feedback resistors of the Bern Isoprime machine; the thick line represents that part of the continuous beam which becomes finally collected in the respective Faraday cups (vertical dashed lines mark the geometric limits of the Faraday cups as a visualisation of the spatial integration of the Faraday cup).

Using this concept of two individual contributions to the total Kr signal, one can explain the following observations:

- pure Kr produces signals at nominal m/z 44 and higher
- the magnitude of the Kr interference depends on the mass spectrometer
- the focusing parameters of the ion source can alter the interferences
- at stable focusing conditions, the effects on $\delta^{13}\text{C}$ and $\delta^{18}\text{O}$ are closely correlated

We want to point out that these observations refer to IRMS measurements in continuous-flow mode where He is admitted continuously to the ion source, leading to a typical pressure of 2×10^{-6} mbar. In dual-inlet mode the source pressure

is about a factor of 10 lower. We have indications from additional tests with dual-inlet IRMS measurements (IMAU), where we admitted Kr without He background, that here the Kr interference is less pronounced. Based on these results we speculate that the m/z 43 ion beam is better focused at dual-inlet conditions, but in continuous-flow mode it is broadened by collisions with He ions in the source or He atoms in the flight tube. A peak broadening during continuous-flow IRMS compared to dual inlet was also observed during stable sulphur isotope analysis using SF_6 (Ono et al., 2006).

5 Solutions for the Kr interference

The observations and experiments discussed above show that Kr can severely interfere with $\delta^{13}\text{C}$ measurements of CH_4 samples if the Kr peak is within the integration boundaries of the CH_4 peak. Given the fact that the Kr interference can produce systematic offsets exceeding the analytical precision, we propose the following strategies to account for or eliminate this effect.

1. GC separation of Kr from CH_4 prior to conversion to CO_2
2. GC separation of Kr from CO_2 after the CH_4 -to- CO_2 conversion
3. Cryogenic separation of Kr from CO_2 after the CH_4 -to- CO_2 conversion
4. Raw beam time series correction using anomalies in the ion current ratios
5. Early peak cut-off at the right integration boundary
6. Correction using relations between $\delta 45$ and $\delta 46$

It is beyond the scope of this paper to discuss all strategies in great detail. Separate technical papers will deal with the individual solutions applied to a particular system. Instead, we want to provide an overview of possible solutions to let the reader make a first selection on the preferred strategy. The six strategies fall into two classes. Strategies 1 to 3 are technical solutions, which prevent the peak overlap in the ion source and thus avoid the Kr interference for new measurements. Strategies 4 to 6 allow correcting existing data sets. These correction strategies were specifically developed for the existing data sets of our respective systems. As the four systems show different characteristics of the Kr interference, these correction strategies cannot be applied interchangeably. Consequently, we could not compare the performance of the three correction approaches, but discuss their strengths and limitations individually.

5.1 GC separation of Kr from CH_4

Of all the proposed solutions in this section, the chromatographic separation of CH_4 from Kr seems to be the most

elegant and straightforward way since no additional device is needed besides the basic setup described by Merritt et al. (1995). The only requirement is that the chromatographic separation is good enough to allow a sufficient separation of CH_4 and Kr. Without knowing that Kr was the “unknown contaminant peak”, Rice et al. (2001) were the first to master this problem with a cryo-GC at -50°C . To maintain narrow peak width, they used high flow rates of 2.6 mL min^{-1} , thus a factor 2.5 higher than typically used for ice core analyses. This approach is also applied by others (Umezawa et al., 2009). Schaefer and Whiticar (2007) followed the same route and used a sub-ambient GC at 0°C to separate what they call N_2O . However, they concluded that separation at 0°C was insufficient, and a second GC column was introduced after the combustion oven.

With the Bern system, we tested the option to better separate CH_4 from Kr using lower GC temperatures. For the experiments we used a 30 m PoraPLOT column at a flow rate of ca. 1 mL min^{-1} and measured the chromatographic separation between CH_4 and Kr for three temperatures: 5, 18, and 30°C . A Kr–He mixture was injected onto the GC flow and cryofocused (Fig. 1). Measurements were made under CO_2 focusing conditions. We did not inject CH_4 but used the small amount of CH_4 cryofocused as blank contribution. This small CH_4 amount turned out to be ideal for these experiments as an amount of CH_4 comparable to samples would otherwise overwhelm the Kr peak. The results are shown in Fig. 8. For 30°C (Fig. 8a) the separation is only 8 s – thus, insufficient – and results in comparable retention time differences to the CarbonPLOT column (ca. 6 s). A reduction to 5°C (Fig. 8c) shows that the separation of CH_4 from Kr is much better and amounts to 16 s, allowing Kr-free $\delta^{13}\text{C}$ analysis of CH_4 . However, this low GC temperature had the disadvantage that N_2O eluted very late and showed a very broad peak shape, which is not suitable for isotope analysis on N_2O . Since in our ice core analysis we measure $\delta^{13}\text{C}$ and N_2O isotopes in the same run, we did not choose this route but decided to follow the route described in Sect. 5.3.

5.2 Chromatographic separation after the CH_4 - CO_2 conversion

The following section describes the separation of Kr from the combusted CH_4 peak using a post-combustion GC column. As shown above and from other studies (Rice et al., 2001), a sufficient separation of CH_4 from Kr requires low GC temperatures due to similar physico-chemical properties of CH_4 and Kr on the GC column. However, after the combustion oven the resulting CO_2 is relatively easy to separate from Kr since already at ambient temperatures (e.g. 30°C) Kr elutes much earlier than CO_2 on regular GC columns.

The usage of a post-combustion GC column for $\delta^{13}\text{C}$ of CH_4 was first described in Schaefer and Whiticar (2007), who included this device to separate what they interpreted as N_2O . In the following, we show results from the updated

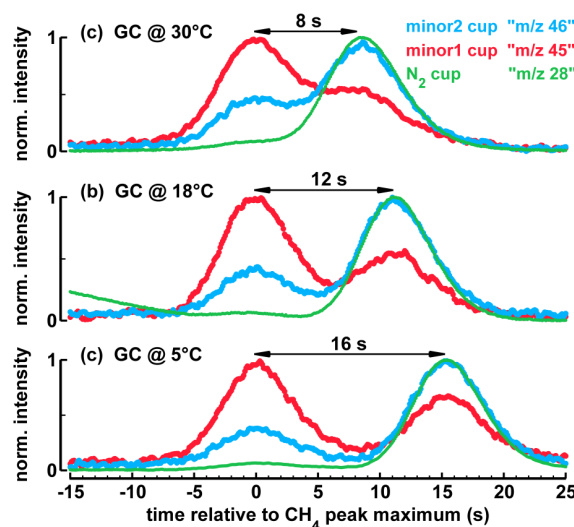


Fig. 8. Chromatograms showing the separation between CH_4 (left peak) and Kr (right peak) on a PoraPLOT column for 30°C , 18°C and 5°C measured with the Bern system. The Kr interference is visible in all Faraday cups, either as a direct signal of $^{84}\text{Kr}^{3+}$ in the m/z 28 cup (thin green line) or from the broad Kr interference for the minor1 and minor2 (thick red and blue, respectively).

IMAU $\delta^{13}\text{C}$ system, where also a post-conversion GC column is used to avoid the Kr interference (Fig. 1). The additional component consists of a 12.5 m piece of PoraPlotQ column in a GC which is operated at 24°C . This GC column was inserted between the Nafion dryer and the open split (see Fig. 1 in Sapart et al., 2011) and provides a separation of Kr from CO_2 (CH_4) of about 30 s (Fig. 9b). The figure also nicely shows the response of the IMAU mass spectrometer to pure Kr resulting in a very pronounced peak on the minor2 cup collecting the nominal m/z 46 ions. A much smaller peak can be seen on minor1 cup (nominal m/z 45). This observation fits with the experiments where pure Kr was added to an air sample and a strong enrichment for $\delta^{18}\text{O}$ was observed while the enrichment for $\delta^{13}\text{C}$ was smaller (7.2 ‰ for $\delta^{18}\text{O}$, and 0.79 ‰ for $\delta^{13}\text{C}$ per 1 ppm Kr added). In contrast to the Bern system, here the Kr signal on the major cup $< 0.1\text{ mV}$ is too small to be visible; thus, the intensities on minor1 and minor2 become fully expressed as anomalies, leading to the strong biases in $\delta^{13}\text{C}$ and $\delta^{18}\text{O}$ observed for the original IMAU system (compare with the Bern system, Figs. 4, 5 and 10).

To assess the overall performance of the updated IMAU system, the three intercomparison cylinders which were measured with the original IMAU system were remeasured with the updated system as well. A comparison between the original and updated IMAU systems shows that the Kr interference at IMAU amounted to ca. 2.38 ‰ for the GL cylinder, ca. 0.88 ‰ for the PI cylinder and ca. 0.05 ‰ for the PD cylinder (Table 2). The results from the updated IMAU method are also comparable with the measurements

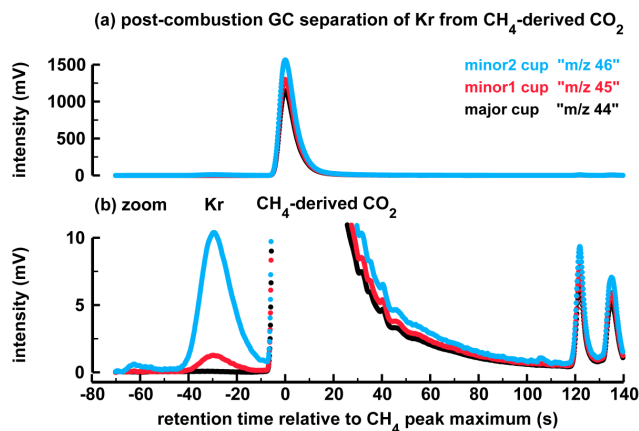


Fig. 9. Chromatogram showing the separation of Kr from CH_4 -derived CO_2 achieved with the improved IMAU system, which includes a GC column after the combustion oven. Due to the additional GC, Kr elutes before instead of after the CH_4 -derived CO_2 peak as shown in the chromatograms of Fig. 3.

obtained at NIWA using dual inlet IRMS, which is free of Kr interference, and with the Kr-corrected results obtained from other labs.

5.3 Cryogenic separation of Kr from CO_2 after the CH_4 - CO_2 conversion

In this section we describe an alternative procedure to separate CO_2 and Kr after the combustion oven, based on the fact that CO_2 can be trapped on a capillary at liquid nitrogen (LN_2) temperature (-196°C) while Kr passes this trap. In the updated Bern system, such a trap is inserted after the combustion oven (post-combustion trap, Fig. 1). Such a trap not only separates CO_2 from Kr but also acts as a cryofocus yielding narrow, high-intensity CO_2 peaks after the capillary is lifted out of the LN_2 (Melton et al., 2011). A second movable trap is inserted before the combustion oven to trap any residual CO_2 from the GC flow (pre-combustion trap, Fig. 1). With the addition of these two traps, Kr now elutes sufficiently earlier (we found 25 s to be a good value) before the sharp CH_4 -derived CO_2 peak, thus providing baseline separation between the two species (Fig. 10). The timing of the post-combustion trap is a critical parameter of this strategy to avoid trapping traces of combusted sample CO. While most of the CO is removed during the first purification step, a small fraction of CO remains and elutes before the CH_4 peak and becomes combusted to CO_2 as well (Fig. 10b). As can be seen in the example chromatogram, the post-combustion trap (trap down arrow in Fig. 10b) is lowered only after the CO-derived CO_2 peak has passed the trap. After a trapping time of 50 s, the capillary is lifted and produces the sharp CO_2 peak. Because Kr is not collected on this capillary, its retention time is basically the same as without the trap. Note that the length of the trapping time should not be unnecessary

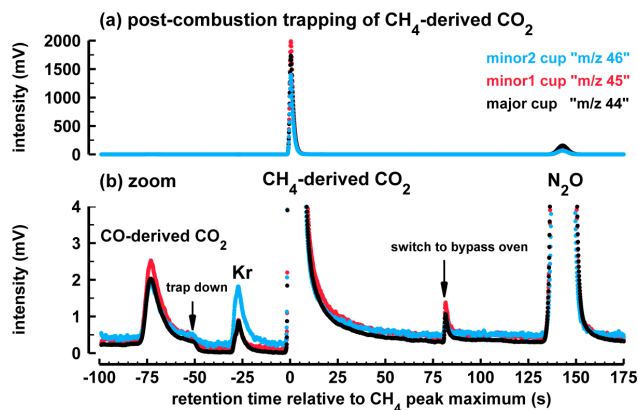


Fig. 10. Sample chromatogram showing the separation of Kr from CH_4 -derived CO_2 for the improved Bern system. (a) Full-range plot of the narrow, cryofocused, CH_4 -derived CO_2 peak and the broader N_2O peak without the cryofocusing step. (b) Zoomed plot to see the separation of Kr from CH_4 -derived CO_2 . The arrow “trap down” marks the time when the capillary is lowered into LN_2 to trap the CO_2 from the combustion oven. While CO_2 becomes trapped at LN_2 temperature, Kr passes the capillary without delay and shows the typical Kr interference signal.

long since CO_2 bleeding from the combustion oven adds up to blank contribution, which has to be minimised. After the CO_2 peak is measured by the IRMS, a valve is switched to allow the N_2O peak to bypass the combustion oven (Fig. 1, green circles). Note the different peak shape characteristics of the CH_4 -derived CO_2 peak and the N_2O peak due to the cryofocusing step.

5.4 Subtracting the Kr interference peak from raw data

The above hardware solutions all eliminate the Kr interference. However, extant data sets require an algorithm for correcting for the Kr interference. One method for making the correction relies on the anomalies seen in the ion current ratios, which are particularly pronounced in the data set measured with the AWI system (Fig. 11a). This approach requires the time series of the IRMS acquisition file (raw beam data file) and software to read and process this data (Bock et al., 2010; Schmitt et al., 2011). With a set of equations the signal intensity of the Kr peak is calculated which produced these anomalies in the first place. The time series of these reconstructed Kr interferences are then subtracted from the measured time series to yield the corrected time series. The latter one is then used to calculate the $\delta^{13}\text{C}$ values.

In detail, the correction is based on the following equations, with i representing the time series of an ion current and R the ratio of a pair of ion currents. In the case of the AWI measurements, the time series covers the interval beginning at the CH_4 peak start and extends to 10 s after the maximum of the CH_4 peak (see Fig. 11b). Note that the following equations and explanation only show the correction

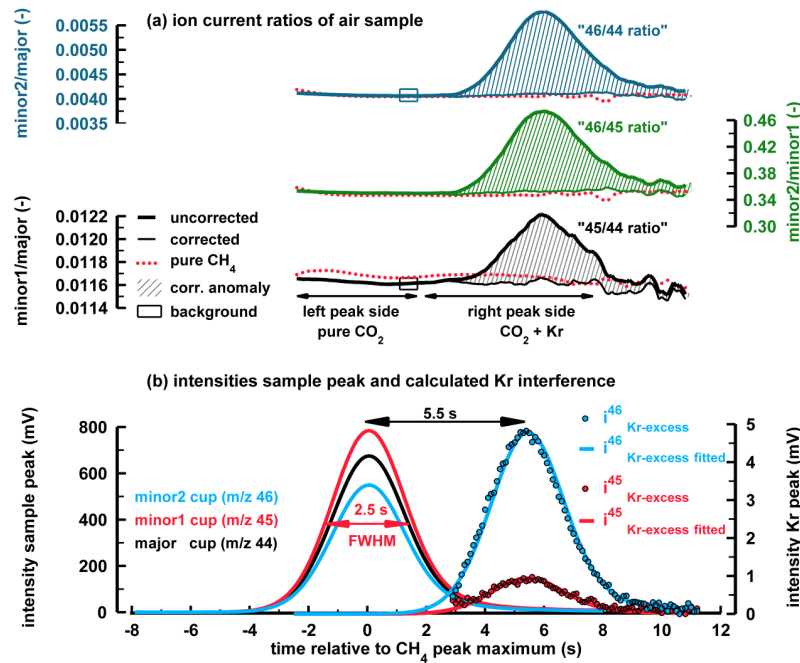


Fig. 11. Compilation showing the principle of the Kr correction for an air sample measured with the AWI system. **(a)** Ion current ratios in bold lines are the uncorrected ratios; the rectangle indicates the time interval that is used to determine the background to calculate the Kr interference shown in the panel below. The thin line and the hatched area show the ratio after the Kr correction, i.e. after the subtraction of the fitted Kr peak from the measured ion current. The red dotted line is the ratio of pure CH₄ without Kr interference. The “46/45 ratio” serves as an independent visual check of whether the correction was successful since the anomaly of this ratio is not used for the correction method. **(b)** Intensities for the three Faraday cups of the CH₄ sample (left axis). The interference calculated from the anomalies plotted in the ratios above (right axis) with the dots representing the calculated raw anomaly for *m/z* 45 and *m/z* 46, the lines are a fit to the respective data used for correction.

of the Kr interference on i^{45} and $R^{45/44}$, the correction for i^{46} is analogous to the i^{45} example. We start by assuming that the CO₂ peak is pure CO₂ in the ion source, i.e. without Kr interference, and the major cup exclusively collects ions, with *m/z* 44 generating the time series of i^{44} , minor1 only *m/z* (i^{45}), and minor2 only *m/z* 46 (i^{46}). In this case, the ion current ratio $R_{\text{measured}}^{45/44}$ is the ratio of the two measured ion currents originating exclusively from CO₂ since i_{measured}^{45} equals $i_{\text{CO}_2}^{45}$ and i_{measured}^{44} equals $i_{\text{CO}_2}^{44}$, given by

$$R_{\text{measured}}^{45/44} = R_{(\text{pure CO}_2)}^{45/44} = i_{\text{CO}_2}^{45} / i_{\text{CO}_2}^{44} = i_{\text{measured}}^{45} / i_{\text{measured}}^{44} \quad (1)$$

However, for a real sample with Kr interference, Eq. (1) is not valid for the entire peak. Instead, the entire CO₂ peak region must be divided into two parts. The left part is dominated by the CO₂ signal and covers the region from ca. 4 s before the CH₄ peak maximum to ca. 2 s after the CH₄ peak maximum (Fig. 11). Equation (1) is only valid for this part. In contrast, the right part is contaminated by Kr. Here, the ion current i_{measured}^{45} is the sum of $i_{\text{CO}_2}^{45}$ and the Kr interference. To generate an anomaly in the ion current ratio of the CO₂ sample, the ion current ratio of the Kr peak must be different from the ion current ratio of the sample. If the ion current ratios of the interfering signals exactly match those of the sample

peak, the $\delta^{13}\text{C}$ and $\delta^{18}\text{O}$ values will be unchanged. For that reason, only the $R^{45/44}$ anomaly to pure CO₂ is calculated in the following equations, with the part of the total i_{Kr}^{45} signal causing this anomaly called $i_{\text{Kr-excess}}^{45}$. The sign of $i_{\text{Kr-excess}}^{45}$ is positive when the minor1/major ratio of the Kr peak is greater than the minor1/major ratio of the pure-CO₂ interval. This case is comparable to the situation of Fig. 5b, left side, with AV < -2 V. Conversely, $i_{\text{Kr-excess}}^{45}$ can be negative for cases resembling the situation in Fig. 5b, right side, with AV > -1 V. Therefore, for the right side of the peak, Eq. (1) is not valid, since $R_{\text{measured}}^{45/44}$ is the sum of $i_{\text{CO}_2}^{45}$ and $i_{\text{Kr-excess}}^{45}$ divided by i_{measured}^{44} :

$$R_{\text{measured}}^{45/44} = R_{(\text{CO}_2+\text{Kr})}^{45/44} = (i_{\text{CO}_2}^{45} + i_{\text{Kr-excess}}^{45}) / i_{\text{measured}}^{44} \quad (2)$$

The next step relies on the observation gleaned from the AWI data that all three ion current ratios of pure-CH₄-derived CO₂ peaks are essentially flat. In contrast, the ratios of the affected sample peaks show large Kr bumps after the flat plateaus due to Kr signals (Figs. 11a and 2d–f). To calculate a quantitative measure of the Kr interference on the ion current ratio, the absolute anomaly of these Kr bumps, $\Delta R^{45/44}$, is defined as follows:

$$\Delta R^{45/44} = R_{(\text{CO}_2+\text{Kr})}^{45/44} - R_{(\text{pure CO}_2)}^{45/44} \quad (3)$$

In practice, $\Delta R^{45/44}$ is calculated by subtracting the “background ratio” defined as $i_{\text{CO}_2}^{45}/i_{\text{measured}}^{44}$, from the ratio of the affected right peak side with the contaminated ratio, $R_{(\text{CO}_2+\text{Kr})}^{45/44}$. The peak section from which the “background ratio” is calculated is indicated by boxes in Fig. 11a. At this step we make the assumption that without any Kr interference the ratio in the background box would continue all the way to the right side, to the right integration boundary (8 to 10 s after CH₄ peak maximum). This assumption is reasonable at this step for defining the “background ratio” since pure-CH₄ peaks show an almost flat ratio over the whole CH₄ peak (see Figs. 2d–f and 11a).

Equation (3) can be transformed into Eq. (4), into Eq. (5) and finally into Eq. (6) where the ion current of the excess Kr, $i_{\text{Kr-excess}}^{45}$, is isolated.

$$\Delta R^{45/44} = (i_{\text{CO}_2}^{45} + i_{\text{Kr-excess}}^{45})/i_{\text{measured}}^{44} - i_{\text{CO}_2}^{45}/i_{\text{measured}}^{44} \quad (4)$$

$$\Delta R^{45/44} = i_{\text{Kr-excess}}^{45}/i_{\text{measured}}^{44} \quad (5)$$

$$i_{\text{Kr-excess}}^{45} = \Delta R^{45/44} \cdot i_{\text{measured}}^{44} \quad (6)$$

The $i_{\text{Kr-excess}}^{45}$ time series resembles a Gaussian peak shape with its maximum at the retention time of the Kr peak (Fig. 11b, blue dots), which indicates that the method allows extracting the Kr interference. Before continuing the calculation, we want to point out the counterintuitive temporal offset between the maximum of the Kr peak and the anomaly maximum of ion current ratio visible in Figs. 2, 4 and 11. Typically, the maximum of the Kr peak occurs a few seconds earlier than the maximum in the ion current ratio. Theoretically, if both the CH₄-derived CO₂ peak and the Kr peak were ideally Gaussian, the background-corrected ion current ratio on the right side of the Kr peak should asymptotically approach the respective ion current ratio of the Kr peak itself. However, the ion current ratio usually shows a local maximum a few seconds after the maximum of the Kr peak and then declines towards the value of the CO₂. Our interpretation is that both peaks are non-Gaussian and CO₂ has a longer residence time in the ion source and in the capillaries due to adsorption effects compared to the noble gas krypton. For that reason the measured ion current ratio in the region of the declining flank of the Kr peak becomes progressively dominated by CO₂. The $i_{\text{Kr-excess}}^{45}$ is not directly used for the correction but a fit to this time series. This fit is called $i_{\text{Kr-excess}}^{45 \text{ fitted}}$. The fit is more accurate and more robust to the selected “background ratio” used in Eq. (3) than the raw $i_{\text{Kr-excess}}^{45}$ time series, and the entire Kr peak can be subtracted (see Fig. 11b). The fit is obtained by scaling the CH₄-derived CO₂ peak with the height of the $i_{\text{Kr-excess}}^{45}$ peak using the observation that a Kr peak and a CH₄-derived CO₂ peak are of almost congruent peak shape. Accordingly, the fitting step aims to extract only the part of the $\Delta R^{45/44}$ anomaly that can be related to a Kr peak (Fig. 11b); for details see the corrected minor1/major ratio (thin line, Fig. 11a) which is not a flat line as would be

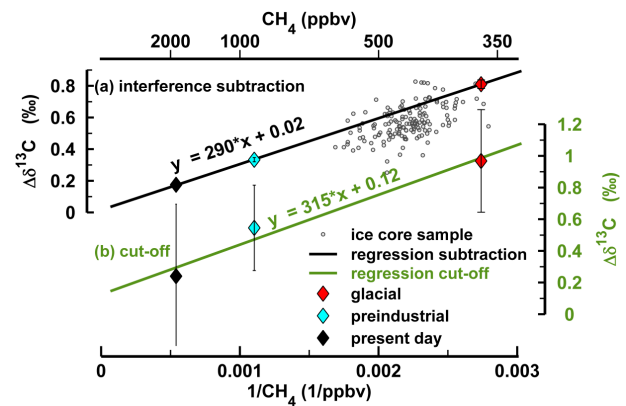


Fig. 12. Comparison of two methods to account for the Kr interference based on measurements with the AWI system using the three intercomparison cylinders with contrasting CH₄/Kr mixing ratios. Plotted are the $\Delta\delta^{13}\text{C}$ numbers, i.e. the differences between the original results and the results obtained after removing the Kr effect. Both methods reveal that with decreasing CH₄ concentrations (hence, CH₄/Kr mixing ratios) $\Delta\delta^{13}\text{C}$ becomes larger. **(a)** Results for the method of Sect. 5.4, where the Kr interference is subtracted from the raw data time series. Coloured diamonds with error bars mark the cylinder measurements; grey circles show a data set of 152 ice core measurements. **(b)** Results for the relatively simple method, where the right integration boundary is shifted from 10 to 3 s after the CH₄ peak maximum to cut off a large fraction of the Kr peak. This method is more vulnerable to peak shape variations leading to more noise in the results.

the case if the full $\Delta R^{45/44}$ (raw anomaly) had been removed (Fig. 11a). Using $i_{\text{Kr-excess}}^{45 \text{ fitted}}$ the measured time series can be corrected as follows:

$$i_{\text{corrected}}^{45} = i_{\text{measured}}^{45} - i_{\text{Kr-excess}}^{45 \text{ fitted}} \quad (7)$$

These equations provide a quantitative way to correct for the Kr interference measured on the minor1 cup. To correct the interference on the minor2 cup, equivalent equations for i^{46} have to be solved. The corrected time series are then fed into our peak integration software to determine the peak areas within the integration limits of the CH₄-derived CO₂ peak and finally the $\delta^{13}\text{C}$ value. We have applied this correction to results from the intercalibration cylinders with contrasting CH₄ mixing ratios (CH₄/Kr ratios) to demonstrate how the interference scales with CH₄ mixing ratio and to estimate the precision of this correction (Fig. 12a). We see a close linear relationship between the absolute correction, $\Delta\delta^{13}\text{C}$, and the inverse CH₄ mixing ratio ($1/\text{CH}_4$) with $\Delta\delta^{13}\text{C}$ values of only 0.18 ‰ for the “present day” cylinder, 0.33 ‰ for the “pre-industrial” cylinder and 0.81 ‰ for the “glacial” cylinder of the round-robin exercise. The standard deviation of the absolute correction, $\Delta\delta^{13}\text{C}$ values, averaged over the three cylinders is 0.02 ‰; thus, the correction algorithm adds only little noise to the measurement noise of the results.

In principle, this close linear relationship seen in Fig. 12a can be exploited to correct samples with known CH₄ mixing

ratio in the sense of applying a calibration curve to samples. This approach could be valuable, if samples cannot be corrected individually with the above-described algorithm. To evaluate this route, Fig. 12a additionally shows the results from a large data set of ice core samples which were measured with the AWI system. Here we see that the individually corrected samples show a similar CH₄ dependency to the results from the cylinder measurements, yet the correlation is much weaker. The weaker correlation and the scatter around the regression line of the cylinder results do not reflect the correction method itself; the scatter is rather due to the temporal variability of the Kr effect. While the cylinder measurements were obtained within a few weeks, the ice core data set was measured over a period of two years with some changes in the source focusing parameters. From this we can conclude that if the relation of $\Delta\delta^{13}\text{C}$ vs. $1/\text{CH}_4$ is used for correcting affected samples, this can be done very precisely when the calibration measurements are done in close proximity to the sample measurements. On the contrary, additional noise is added to the data when measurement and calibration are not performed at the same instrument conditions, as the relation of $\Delta\delta^{13}\text{C}$ vs. $1/\text{CH}_4$ is subject to changes over time.

5.5 Early peak cut-off

Another method for correcting extant data for Kr may be employed when there is sufficient separation between the Kr and CH₄ peaks. The relative position of the Kr and CH₄ peaks must first be determined as discussed in Sect. 4.1. Once the position of the Kr peak has been established, one can determine when to cut off the CH₄ peak in order to minimise the Kr interference. There is a trade-off involved in removing larger portions of the Kr interference as that requires larger portions of the sample peak to be removed as well. If we assume that the total Kr effect on $\delta^{13}\text{C}$ for a sample amounts to 0.8‰, a 90% cut-off of the Kr peak brings the remaining interference to 0.08‰, i.e. already below the usual measurement precision of ca. 0.1 to 0.2‰. With this approach most of the Kr peak is removed, while only about 10% of the CH₄ peak is lost. In the case of the AWI measurements this translates to a right integration boundary position of 3 s after CH₄ peak maximum. Clearly, this approach violates the rule that the entire peak must be used for isotope analysis, but this can be accommodated by the identical treatment principle (Werner and Brand, 2001). The consequences can be seen in Fig. 12b. The price for this cut is a higher noise level of ca. 0.35‰ and a systematic bias of ca. 0.2‰ which results from systematic differences of the isotopic ratio along the peak. The results of this simple cutting approach could be improved when a certain peak fraction, i.e. 10%, is cut off instead of a fixed time as used here to accommodate for peak shape changes in different chromatograms.

The simplicity of this approach allows for a first check of whether and to what extent the $\delta^{13}\text{C}$ data might be influenced by the Kr interference. It also provides confidence

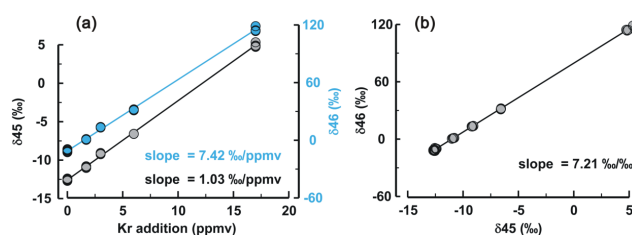


Fig. 13. Results of artificially adding pure Kr to a CH₄ sample. **(a)** Both isotope ratios show a linear relation of the δ values with the amount of Kr added. **(b)** The isotope ratios are closely correlated ($r^2 = 1.00$) and this relation can be used to correct for the Kr interference without knowing the exact CH₄-Kr mixing ratio of a sample. Note that here the δ_{46}/δ_{45} slope is shown, i.e. the inverse value used in Eq. (9).

in the more sophisticated correction algorithm presented in Sect. 5.4 as it yields a correction of similar magnitude. We applied both the cut-off technique and the subtraction technique on the large ice core data set measured at AWI and conclude that both correction techniques provide similar $\delta^{13}\text{C}$ -corrected values (data not shown).

5.6 Correction using relations between δ_{45} and δ_{46}

The following section describes a correction routine applied by IMAU. The basis for this correction approach is the fact that the Kr interference affects both the minor1 and the minor2 cup, thus δ_{45} ($\delta^{45/44}$) and δ_{46} ($\delta^{46/44}$) as shown in Fig. 13. This leads to biases for both $\delta^{13}\text{C}$ and $\delta^{18}\text{O}$, which show a tight linear relation (e.g. Fig. 5).

A necessary prerequisite to using the δ_{45}/δ_{46} relation for correction is the fact that the $\delta^{18}\text{O}$ of the combustion product CO₂ is very similar for sample and reference air peaks. This is usually the case because all oxygen atoms of CO₂ are derived from O₂ during the combustion process. Consequently, the $\delta^{18}\text{O}$ deviation of a Kr-affected sample from a pure-CH₄ sample can be ascribed to the influence of the Kr interference on $\delta^{13}\text{C}$. Note that this assumption is only valid if sample and the pure CH₄ are measured closely together, at least on the same day; otherwise the $\delta^{18}\text{O}$ values are subject to long-term drift caused by the redox state of the combustion furnace. To apply this correction, the relation of δ_{45}/δ_{46} for the Kr interference has to be acquired. For this, we used the results from the experiments where increasing amounts of Kr were added to a CH₄ sample (Sect. 3). For the correction, the following equation is used:

$$\delta^{13}\text{C}_{\text{corrected}} = \delta^{13}\text{C}_{\text{measured}} - (\delta^{18}\text{O}_{\text{sample}} - \delta^{18}\text{O}_{\text{reference}}) \cdot \text{slope}_{\delta_{45}/\delta_{46}} \quad (8)$$

where $\delta^{13}\text{C}_{\text{corrected}}$ is the $\delta^{13}\text{C}$ value after correction, $\delta^{13}\text{C}_{\text{measured}}$ is the raw measured value, $\delta^{18}\text{O}_{\text{sample}}$ and $\delta^{18}\text{O}_{\text{reference}}$ are the $\delta^{18}\text{O}$ values of the sample and a bracketing reference measurement of pure CH₄, and $\text{slope}_{\delta_{45}/\delta_{46}}$ is the slope of the experiments from Sect. 3 (see Fig. 13).

The value used for the slope is $\delta^{45}/\delta^{46} = 0.1388 \pm 0.0008\%$, or approximately 0.14‰ in $\delta^{13}\text{C}$ for 1‰ in $\delta^{18}\text{O}$. Note that for samples the introduced error stemming from the uncertainty of the slope is small and scales with the CH_4/Kr mixing ratio. As an example, for a sample which is corrected by 1.39‰, a typical value for glacial ice samples, the error due to the slope amounts to only 0.008‰ and, thus, is small compared to the analytical uncertainty of ca. 0.1 to 0.2‰. A second type of error results from the measurement uncertainty of $\delta^{18}\text{O}$ for both the sample and the reference. Ideally, the measured $\delta^{18}\text{O}$ values for samples and references should only deviate due to the Kr interference and should be equal for Kr-free CH_4 samples. However, the $\delta^{18}\text{O}$ values might vary over time since the conditions of the combustion furnace can change with time. Depending on how and in which intervals the furnace is reoxidised with O_2 , the variability of $\delta^{18}\text{O}$ is dependent on the system used and should be checked before this correction technique is used to correct a measured data set of $\delta^{13}\text{C}$. Moreover, changes in the IRMS source focusing may change the slope over time. The advantage of this method is that it does not involve special software to do the raw data correction as described in Sect. 5.4. To calibrate this correction, it would suffice to have two gases with known and different CH_4/Kr ratio.

Again, the results from the three intercomparison cylinders provide the means to assess the Kr correction. The comparison of Kr-corrected $\delta^{13}\text{C}$ values measured with the original IMAU method and measurements with the updated IMAU system shows that the Kr-corrected values are very close to the results from the updated IMAU system and the dual-inlet measurement of NIWA (Table 2).

6 Summary and conclusions

This paper identified for the first time that Kr can severely interfere with the measurement of $\delta^{13}\text{C}$ of CH_4 during CF-IRMS analysis. The interference for $\delta^{13}\text{C}$ can be as large as 2‰ if samples are measured which have high Kr-to- CH_4 ratios, e.g. air extracted from ice core samples or stratospheric samples, relative to modern atmospheric air as reference gas. In the ion source of the mass spectrometer the krypton isotope ^{86}Kr produces doubly charged ions with a m/z of 43. We demonstrate that the lateral tail of this beam extends into the major and partly also into the minor1 cup, compromising the measured m/z 44 and m/z 45 signal. We speculate that the rather flat Kr interference observed in the minor2 cup (m/z 46) either results from a further extension of this $^{86}\text{Kr}^{2+}$ tail or is due to reflections of the more abundant singly charged Kr ions. As a result, all three Faraday cups used for $\delta^{13}\text{C}$ analysis are affected by the Kr interference. The sign and magnitude of this bias is specific for the used instrument and is dependent on the focusing; thus, the bias can change over time. In this sense, the Kr interference can

lead to incorrect values, concentration effects (scale effects), and drifts over time and can simply increase the measurement noise. At constant instrument conditions, the $\delta^{13}\text{C}$ bias of atmospheric CH_4 samples inversely scales with the CH_4 mixing ratio since the Kr mixing ratio can be regarded as constant. For example, air samples with lower CH_4 mixing ratios will yield higher (heavier) apparent $\delta^{13}\text{C}$ values compared to samples with higher CH_4 mixing ratios. In the second part of the paper we presented several strategies to tackle the Kr problem. Existing methods can be adapted to separate Kr from CH_4 either before the combustion process or after conversion to CO_2 . For existing data sets we propose several correction methods to account for the Kr interference.

Regarding the implications of this effect, we identified the following fields of research using $\delta^{13}\text{C}$ of CH_4 where the Kr interference could be relevant if it is not taken into account. The Kr interference is relevant if high accuracy in $\delta^{13}\text{C}$ is needed and/or samples with low CH_4/Kr ratio mixing ratios are analysed. Note that round-robin intercomparison studies aimed to identify offsets between laboratories cannot solve this issue if pure- CH_4 standards, synthetic-air mixtures (N_2 , O_2) or real samples with only one CH_4/Kr ratio are distributed. Examples for such studies are as follows:

- Palaeo-atmospheric studies on air with low CH_4/Kr mixing ratios (atmospheric CH_4 mixing ratios as low as 360 ppb), e.g. during the glacial period.
- Current atmospheric studies in settings where the atmospheric CH_4/Kr mixing ratio is considerably lowered due to a loss process (e.g. high-stratospheric air samples, microbial oxidation in aerobic soil layers).
- High-precision and -accuracy studies of recent atmospheric $\delta^{13}\text{CH}_4$. Note that since the late 1990s when many $\delta^{13}\text{CH}_4$ long-term measurements started, by coincidence the atmospheric CH_4 mixing ratio has remained unusually stable.
- Studies analysing the interhemispheric gradient of $\delta^{13}\text{C}$ which rely on measurements from different measurement systems.
- Fresh or sea water samples which had atmospheric contact having low CH_4/Kr mixing ratios due to higher solubility of Kr compared to CH_4 .

The compilation shows that the Kr interference is most relevant for the atmospheric community since the demand on accuracy is often high. However, $\delta^{13}\text{C}$ analyses on CH_4 in other sample matrices could be biased by this effect as well. In the case of natural-water samples which equilibrated with the atmosphere, the higher solubility of Kr relative to CH_4 (about a factor of 1.8) leads to a lower CH_4/Kr ratio for the dissolved gases in the water phase. In settings where CH_4 is consumed by methane oxidising bacteria (e.g. deep-water samples), CH_4/Kr mixing ratios can approach values as low

as $0.1 \text{ (nmol nmol}^{-1}\text{)}$ (Heeschen et al., 2004). Like for other types of studies where the fractionation factor of a sink process is analysed (e.g. stratospheric samples), any covariation between the CH_4 concentration and an erroneously measured $\delta^{13}\text{C}$ finally translates into an erroneous assessment of the fractionation factor α .

The described effect in this paper could also be relevant for other precise measurements using IRMS, where the gas matrix of sample and standard are different and a variable component produces a large beam with a m/z close to a target mass of the analysed species.

Acknowledgements. The work at Bern was supported by the University of Bern, the Swiss National Science Foundation, and the ERC advanced grant project “MATRICS”. The work at Utrecht University was funded by the Dutch Science Foundation (NWO) (Projects: 851.30.020 & 865.07.001). TAS support for this research came from NSF 0944584. We would like to thank Hinrich Schaefer for generously sharing the NIWA measurements of the round-robin cylinder intercomparison shown in Table 2. We also thank Jeff Severinghaus, Willi Brand and Hinrich Schaefer for their constructive and very helpful comments on the discussion version of this paper, which improved this paper considerably.

Edited by: P. Herckes

References

- Aoki, N. and Makide, Y.: The concentration of krypton in the atmosphere – Its revision after half a century, *Chem. Lett.*, 34, 1396–1397, doi:10.1246/cl.2005.1396, 2005.
- Behrens, M., Schmitt, J., Richter, K.-U., Bock, M., Richter, U., Levin, I., and Fischer, H.: A gas chromatography/combustion/isotope ratio mass spectrometry system for high-precision $\delta^{13}\text{C}$ measurements of atmospheric methane extracted from ice core samples, *Rapid Commun. Mass Sp.*, 22, 3261–3269, doi:10.1002/rcm.3720, 2008.
- Bergamaschi, P., Bräunlich, M., Marik, T., and Brenninkmeijer, C. A. M.: Measurements of the carbon and hydrogen isotopes of atmospheric methane at Izana, Tenerife: Seasonal cycles and synoptic-scale variations, *J. Geophys. Res.-Atmos.*, 105, 14531–14546, doi:10.1029/1999JD901176, 2000.
- Bock, M., Schmitt, J., Behrens, M., Möller, L., Schneider, R., Sapart, C., and Fischer, H.: A gas chromatography/pyrolysis/isotope ratio mass spectrometry system for high-precision δD measurements of atmospheric methane extracted from ice cores, *Rapid Commun. Mass Sp.*, 24, 621–633, doi:10.1002/rcm.4429, 2010.
- Bousquet, P., Ciais, P., Miller, J. B., Dlugokencky, E. J., Hauglustaine, D. A., Prigent, C., Van der Werf, G. R., Peylin, P., Brunke, E. G., Carouge, C., Langenfelds, R. L., Lathiere, J., Papa, F., Ramonet, M., Schmidt, M., Steele, L. P., Tyler, S. C., and White, J.: Contribution of anthropogenic and natural sources to atmospheric methane variability, *Nature*, 443, 439–443, doi:10.1038/nature05132, 2006.
- Brass, M. and Röckmann, T.: Continuous-flow isotope ratio mass spectrometry method for carbon and hydrogen isotope measurements on atmospheric methane, *Atmos. Meas. Tech.*, 3, 1707–1721, doi:10.5194/amt-3-1707-2010, 2010.
- Bräunlich, M., Aballanin, O., Marik, T., Jockel, P., Brenninkmeijer, C. A. M., Chappellaz, J., Barnola, J. M., Mulvaney, R., and Sturges, W. T.: Changes in the global atmospheric methane budget over the last decades inferred from ^{13}C and D isotopic analysis of Antarctic firn air, *J. Geophys. Res.-Atmos.*, 106, 20465–20481, doi:10.1029/2001JD900190, 2001.
- Burford, J. R. and Bremner, J. M.: Gas chromatographic determination of carbon dioxide evolved from soils in closed systems, *Soil Biol. Biochem.*, 4, 191–197, 1972.
- Craig, H.: Isotopic standards for carbon and oxygen and correction factors for mass-spectrometric analysis of carbon dioxide, *Geochim. Cosmochim. Acta*, 12, 133–149, 1957.
- Deines, P.: Mass spectrometer correction factors for the determination of small isotopic composition variations of carbon and oxygen, *Int. J. Mass Spectro. Ion Phys.*, 4, 283–295, 1970.
- Deniff, S., Gstir, B., Hanel, G., Feketeova, L., Matejcek, S., Becker, K., Stamatovic, A., Scheier, P., and Mark, T. D.: Multiple ionization of helium and krypton by electron impact close to threshold: appearance energies and Wannier exponents, *J. Phys. B.*, 35, 4685–4694, doi:10.1088/0953-4075/35/22/310, 2002.
- Fallick, A. E. and Baxter, M. S.: Pressure Effect and Peak Broadening in Gas Source Stable Isotope Mass-Spectrometry, *Int. J. Mass Spectro. Ion Process.*, 25, 155–165, doi:10.1016/0020-7381(77)80046-6, 1977.
- Ferretti, D. F., Miller, J. B., White, J. W. C., Etheridge, D. M., Lassey, K. R., Lowe, D. C., Meure, C. M. M., Dreier, M. F., Trudinger, C. M., van Ommen, T. D., and Langenfelds, R. L.: Unexpected changes to the global methane budget over the past 2000 years, *Science*, 309, 1714–1717, doi:10.1126/science.1115193, 2005.
- Fischer, H., Behrens, M., Bock, M., Richter, U., Schmitt, J., Loulergue, L., Chappellaz, J., Spahni, R., Blunier, T., Leuenberger, M., and Stocker, T. F.: Changing boreal methane sources and constant biomass burning during the last termination, *Nature*, 452, 864–867, doi:10.1038/nature06825, 2008.
- Francey, R. J., Manning, M. R., Allison, C. E., Coram, S. A., Etheridge, D. M., Langenfelds, R. L., Lowe, D. C., and Steele, L. P.: A history of delta $\delta^{13}\text{C}$ in atmospheric CH_4 from the Cape Grim Air Archive and Antarctic firn air, *J. Geophys. Res.-Atmos.*, 104, 23631–23643, doi:10.1029/1999JD900357, 1999.
- He, B., Olack, G. A., and Colman, A. S.: Pressure baseline correction and high-precision CO_2 clumped-isotope (Δ_{47}) measurements in bellows and micro-volume modes, *Rapid Commun. Mass Spectrom.*, 26, 2837–2853, doi:10.1002/rcm.6436, 2012.
- Headly, M. A. and Severinghaus, J. P.: A method to measure Kr/ N_2 ratios in air bubbles trapped in ice cores and its application in reconstructing past mean ocean temperature, *J. Geophys. Res.-Atmos.*, 112, D19105, doi:10.1029/2006JD008317, 2007.
- Heeschen, K. U., Keir, R. S., Rehder, G., Klatt, O., and Suess, E.: Methane dynamics in the Weddell Sea determined via stable isotope ratios and CFC-11, *Global Biogeochem. Cy.*, 18, GB2012, doi:10.1029/2003GB002151, 2004.
- Kai, F. M., Tyler, S. C., Randerson, J. T., and Blake, D. R.: Reduced methane growth rate explained by decreased Northern Hemisphere microbial sources, *Nature*, 476, 194–197,

- doi:10.1038/nature10259, 2011.
- Keppeler, F., Hamilton, J. T. G., Brass, M., and Röckmann, T.: Methane emissions from terrestrial plants under aerobic conditions, *Nature*, 439, 187–191, doi:10.1038/nature04420, 2006.
- King, S. J. and Price, S. D.: Electron ionization of CO₂, *Int. J. Mass Spectrom.*, 272, 154–164, doi:10.1016/j.ijms.2008.02.008, 2008.
- Leckrone, K. J. and Hayes, J. M.: Water-Induced Errors in Continuous-Flow Carbon Isotope Ratio Mass Spectrometry, *Anal. Chem.*, 70, 2737–2744, doi:10.1021/ac9803434, 1998.
- Levin, I., Veidt, C., Vaughn, B. H., Brailsford, G., Bromley, T., Heinz, R., Lowe, D., Miller, J. B., Poss, C., and White, J. W. C.: No inter-hemispheric $\delta^{13}\text{C}\text{H}_4$ trend observed, *Nature*, 486, E3–E4, doi:10.1038/nature11175, 2011.
- Lowe, D. C., Brenninkmeijer, C. A. M., Tyler, S. C., and Dlugokencky, E. J.: Determination of the Isotopic Composition of Atmospheric Methane and its Application in the Antarctic, *J. Geophys. Res.-Atmos.*, 96, 15455–15467, doi:10.1029/91JD01119, 1991.
- Lowe, D. C., Allan, W., Manning, M. R., Bromley, T., Brailsford, G., Ferretti, D., Gomez, A., Knobben, R., Martin, R., Mei, Z., Moss, R., Koshy, K., and Maata, M.: Shipboard determinations of the distribution of C-13 in atmospheric methane in the Pacific, *J. Geophys. Res.-Atmos.* 104, 26125–26135, doi:10.1029/1999jd900452, 1999.
- Mariotti, A.: Natural N-15 abundance measurements and atmospheric nitrogen standard calibration, *Nature*, 311, 251–252, doi:10.1038/311251a0, 1984.
- Matthews, D. E. and Hayes, J. M.: Isotope-Ratio-Monitoring Gas Chromatography-Mass Spectrometry, *Anal. Chem.*, 50, 1465–1473, doi:10.1021/ac50033a022, 1978.
- Meier-Augenstein, W., Kemp, H. F., and Lock, C. M.: N₂: a potential pitfall for bulk ²H isotope analysis of explosives and other nitrogen-rich compounds by continuous-flow isotope-ratio mass spectrometry, *Rapid Commun. Mass Spectrom.*, 23, 2011–2016, doi:10.1002/rcm.4112, 2009.
- Melton, J. R., Whiticar, M. J., and Eby, P.: Stable carbon isotope ratio analyses on trace methane from ice samples, *Chem. Geol.*, 288, 88–96, doi:10.1016/j.chemgeo.2011.03.003, 2011.
- Melton, J. R., Schaefer, H., and Whiticar, M. J.: Enrichment in ¹³C of atmospheric CH₄ during the Younger Dryas termination, *Clim. Past*, 8, 1177–1197, doi:10.5194/cp-8-1177-2012, 2012.
- Merritt, D. A., Hayes, J. M., and Des Marais, D. J.: Carbon Isotopic Analysis of Atmospheric Methane by Isotope-Ratio-Monitoring Gas-Chromatography Mass-Spectrometry, *J. Geophys. Res.-Atmos.*, 100, 1317–1326, doi:10.1029/94JD02689, 1995.
- Miller, J. B., Mack, K. A., Dissly, R., White, J. W. C., Dlugokencky, E. J., and Tans, P. P.: Development of analytical methods and measurements of ¹³C/¹²C in atmospheric CH₄ from the NOAA Climate Monitoring and Diagnostics Laboratory global air sampling network, *J. Geophys. Res.-Atmos.*, 107, 4178, doi:10.1029/2001JD000630, 2002.
- Mischler, J. A., Sowers, T. A., Alley, R. B., Battle, M., McConnell, J. R., Mitchell, L., Popp, T., Sofen, E., and Spencer, M. K.: Carbon and hydrogen isotopic composition of methane over the last 1000 years, *Global Biogeochem. Cy.*, 23, GB4024, doi:10.1029/2009GB003460, 2009.
- Möller, L., Sowers, T., Bock, M., Spahn, R., Behrens, M., Schmitt, J., Miller, H., and Fischer, H.: Independent control of methane emissions and isotopic composition over the last 160,000 years, *Nat. Geosci.*, under review, 2013.
- Mook, W. G. and Grootes, P. M.: The Measuring Procedure and corrections for the High-Precision mass-spectrometric analysis of isotopic abundance ratios, especially referring to carbon, oxygen and nitrogen, *Int. J. Mass Spectrom. Ion Phys.*, 12, 273–298, 1973.
- Ono, S., Wing, B., Rumble, D., and Farquhar, J.: High precision analysis of all four stable isotopes of sulfur (³²S, ³³S, ³⁴S and ³⁶S) at nanomole levels using a laser fluorination isotope-ratio-monitoring gas chromatography-mass spectrometry, *Chem. Geol.*, 225, 30–39, doi:10.1016/j.gca.2006.06.1271, 2006.
- Quay, P., Stutsman, J., Wilbur, D., Snover, A., Dlugokencky, E., and Brown, T.: The isotopic composition of atmospheric methane, *Global Biogeochem. Cy.*, 13, 445–461, doi:10.1029/1998GB900006, 1999.
- Rice, A. L., Gotoh, A. A., Ajie, H. O., and Tyler, S. C.: High-Precision Continuous-Flow Measurement of $\delta^{13}\text{C}$ and δD of Atmospheric CH₄, *Anal. Chem.*, 73, 4104–4110, doi:10.1021/ac0155106, 2001.
- Rice, A. L., Tyler, S. C., McCarthy, M. C., Boering, K. A., and Atlas, E.: Carbon and hydrogen isotopic compositions of stratospheric methane: 1. High-precision observations from the NASA ER-2 aircraft, *J. Geophys. Res.-Atmos.*, 108, 4460, doi:10.1029/2002JD003042, 2003.
- Ritz, S. P., Stocker, T. F., and Severinghaus, J. P.: Noble gases as proxies of mean ocean temperature: sensitivity studies using a climate model of reduced complexity, *Quaternary Sci. Rev.*, 30, 3728–3741, doi:10.1016/j.quascirev.2011.09.021, 2011.
- Röckmann, T., Brass, M., Borchers, R., and Engel, A.: The isotopic composition of methane in the stratosphere: high-altitude balloon sample measurements, *Atmos. Chem. Phys.*, 11, 13287–13304, doi:10.5194/acp-11-13287-2011, 2011.
- Santrock, J., Studley, S. A., and Hayes, J. M.: Isotopic analyses based on the mass spectrum of carbon dioxide, *Anal. Chem.*, 57, 1444–1448, 1985.
- Sapart, C. J., van der Veen, C., Vigano, I., Brass, M., van de Wal, R. S. W., Bock, M., Fischer, H., Sowers, T., Buizert, C., Sperlich, P., Blunier, T., Behrens, M., Schmitt, J., Seth, B., and Röckmann, T.: Simultaneous stable isotope analysis of methane and nitrous oxide on ice core samples, *Atmos. Meas. Tech.*, 4, 2607–2618, doi:10.5194/amt-4-2607-2011, 2011.
- Sapart, C. J., Monteil, G., Prokopiou, M., van de Wal, R. S. W., Kaplan, J. O., Sperlich, P., Krumhardt, K. M., van der Veen, C., Houweling, S., Krol, M. C., Blunier, T., Sowers, T., Martinerie, P., Witrant, E., Dahl-Jensen, D., and Röckmann, T.: Natural and anthropogenic variations in methane sources during the past two millennia, *Nature*, 490, 85–88, doi:10.1038/nature11461, 2012.
- Sarma, V., Abe, O., and Saino, T.: Chromatographic separation of nitrogen, argon, and oxygen in dissolved air for determination of triple oxygen isotopes by dual-inlet mass spectrometry, *Anal. Chem.*, 75, 4913–4917, doi:10.1021/ac034314r, 2003.
- Schaefer, H. and Whiticar, M. J.: Measurement of stable carbon isotope ratios of methane in ice samples, *Org. Geochem.*, 38, 216–226, doi:10.1016/j.orggeochem.2006.10.006, 2007.
- Schaefer, H., Whiticar, M. J., Brook, E. J., Petrenko, V. V., Ferretti, D. F., and Severinghaus, J. P.: Ice record of $\delta^{13}\text{C}$ for atmospheric CH₄ across the Younger Dryas-Preboreal transition, *Science*, 313, 1109–1112, doi:10.1126/science.1126562, 2006.

- Schmitt, J., Schneider, R., and Fischer, H.: A sublimation technique for high-precision measurements of $\delta^{13}\text{C}$ and mixing ratios of CO_2 and N_2O from air trapped in ice cores, *Atmos. Meas. Tech.*, 4, 1445–1461, doi:10.5194/amt-4-1445-2011, 2011.
- Schüpbach, S., Federer, U., Kaufmann, P. R., Hutterli, M. A., Burion, D., Blunier, T., Fischer, H., and Stocker, T. F.: A New Method for High-Resolution Methane Measurements on Polar Ice Cores Using Continuous Flow Analysis, *Environ. Sci. Technol.*, 43, 5371–5376, doi:10.1021/es9003137, 2009.
- Sessions, A. L., Burgoyne, T. W., and Hayes, J. M.: Correction of H^3+ contributions in hydrogen isotope ratio monitoring mass spectrometry, *Anal. Chem.*, 73, 192–199, doi:10.1088/0953-4075/35/22/310, 2001.
- Severinghaus, J. P., Grachev, A., Luz, B., and Caillon, N.: A method for precise measurement of argon $40/36$ and krypton/argon ratios in trapped air in polar ice with applications to past firn thickness and abrupt climate change in Greenland and at Siple Dome, Antarctica, *Geochim. Cosmochim. Acta*, 67, 325–343, doi:10.1016/S0016-7037(02)00965-1, 2003.
- Sowers, T.: Atmospheric methane isotope records covering the Holocene period, *Quaternary Sci. Rev.*, 29, 213–221, doi:10.1016/j.quascirev.2009.05.023, 2011.
- Sowers, T., Bernard, S., Aballain, O., Chappellaz, J., Barnola, J. M., and Marik, T.: Records of the $\delta^{13}\text{C}$ of atmospheric CH_4 over the last 2 centuries as recorded in Antarctic snow and ice, *Global Biogeochem. Cy.*, 19, GB2002, doi:10.1029/2004GB002408, 2005.
- Stevens, C. M. and Rust, F. E.: The Carbon Isotopic Composition of Atmospheric Methane, *J. Geophys. Res.-Ocean. Atmos.*, 87, 4879–4882, doi:10.1029/JC087iC07p04879, 1982.
- Tyler, S. C., Ajie, H. O., Gupta, M. L., Cicerone, R. J., Blake, D. R., and Dlugokencky, E. J.: Stable carbon isotopic composition of atmospheric methane: A comparison of surface level and free tropospheric air, *J. Geophys. Res.-Atmos.*, 104, 13895–13910, doi:10.1029/1999JD900029, 1999.
- Tyler, S. C., Rice, A. L., and Ajie, H. O.: Stable isotope ratios in atmospheric CH_4 : Implications for seasonal sources and sinks, *J. Geophys. Res.-Atmos.*, 112, D03303, doi:10.1029/2006JD007231, 2007.
- Umezawa, T., Aoki, S., Nakazawa, T., and Morimoto, S.: A High-precision Measurement System for Carbon and Hydrogen Isotopic Ratios of Atmospheric Methane and Its Application to Air Samples Collected in the Western Pacific Region, *J. Meteorol. Soc. Jpn.*, 87, 365–379, doi:10.2151/jmsj.87.365, 2009.
- Vigano, I., Röckmann, T., Holzinger, R., van Dijk, A., Keppler, F., Greule, M., Brand, W. A., Geilmann, H., and van Weelden, H.: The stable isotope signature of methane emitted from plant material under UV irradiation, *Atmos. Environ.*, 43, 5637–5646, doi:10.1016/j.atmosenv.2009.07.046, 2009.
- Werner, R. A. and Brand, W. A.: Referencing strategies and techniques in stable isotope ratio analysis, *Rapid Commun. Mass Spectrom.*, 15, 501–519, doi:10.1002/rcm.258, 2001.